Carbon materials for Na-S and K-S batteries

Ajay Piriya Vijaya Kumar Saroja[1] and Yang Xu[1,*,†]

[1] Department of Chemistry, University College London, 20 Gordon Street, London WC1H 0AJ, UK

* Correspondence: y.xu.1@ucl.ac.uk

† Lead contact: y.xu.1@ucl.ac.uk

Summary

Global energy demand is rapidly increasing, and it undoubtedly reflets the importance of high-capacity energy storage systems based on earth abundant resources. The practicality of lithium-ion batteries for large-scale energy storage is less likely to be viable due to the limited resources of lithium and their unevenly geographical distribution. Because of the earth abundance of sodium and potassium as well as rich sulphur electrochemistry involving multi-electron transfer, sodium-sulphur (Na-S) and potassium-sulphur (K-S) batteries are promising candidates for large-scale energy storage applications. This review highlights the fundamental battery chemistries and challenges of Na-S and K-S batteries. It discusses the design strategies of cathode, anode, and separator with a focus on the utilisation of carbon materials, highlighting the crucial role of carbon in tackling the challenges. Finally, future perspectives are provided, and plausible directions are outlined for the further advancement of Na-S and K-S batteries.

1. Introduction

Most of the global primary energy is contributed from fossil fuels (83%), and contribution from renewable resources was 12% in 2019.[1] Recognising the consequence of climate change (as seen from the wildfire in the US and Europe and the extreme temperature in western Canada this year) and the urgence of decarbonisation, renewable energy has grabbed global attention and its contribution is expected to increase to 42% in 2050.[1] The total energy storage capacity from both stationary and mobile applications in 2017 was 4.67 TWh and is expected to increase to 15 TWh in 2030 with the increase in the utilisation of renewable energy.[2,3] Therefore, the capacity of grid-connected electric energy storage system (EES) needs to be increased to meet the upcoming demand. Although traditional pumped hydroelectric storage can be used, it has the limitation of a low energy density (0.5 to 1.5 Wh kg^{-1}) and needs geographically suitable locations.[4,5] With regard to EES, batteries are used in load levelling and spinning reserve that requires high energy density, low-self discharge rate, and high round-trip efficiency. Due to these benefits, battery capacity in EES is expected to increase to 167 GWh by 2030 from 11 GWh in 2017.[2,3] Although lithium-ion batteries (LIBs) can satisfy these essential requirements, their utilisation for storing GWh energy is not reliable in terms of the limited resources and cost of their supply materials.[2] The price projection for LIBs for utility application is estimated to be >500 USD kWh^{-1} in 2030, which is much more expensive than conventional pumped hydroelectric storage (~250 USD kWh^{-1}).[6] Other battery technologies such as lead-acid and nickel-cadmium batteries have been used in EES but suffered from low energy density (<70 Wh kg^{-1}), low round trip efficiency (60-80%), and toxicity.[7,6] In this context, alternative high-energy density batteries using abundant resources play a key role for EES in the future.

Based on the two-electron redox reaction of S (S^0 to S^{2-}), metal-S batteries have a high theoretical gravimetric capacity (1675 mAh g^{-1})[9] and energy density, making metal-S batteries a promising energy storage technology for EES, which has been indicated by the well-known

high-temperature Na-S batteries.[10] In recent years, various metal-S batteries operating at room temperature (RT), including Li-S,[11] Na-S,[12] K-S,[13] and Mg-S[14] batteries, have gained significant research interest. Despite the high theoretical energy density of Li-S batteries (2600 Wh kg^{-1}), the low abundance of Li makes it impractical for large-scale storage systems. As the electrochemistry of S with Na^+ and K^+ is very similar to that with Li^+, the integration of widely abundant Na and K (Na: 2.36 wt%; K: 2.09 wt% in the Earth's crust) with S cathode stands out as a good choice compared with other battery technologies **(Figure 1A**). As cost factor is a critical parameter in EES, sacrifice in energy density while moving from Li-S to Na-S and K-S batteries can be compromised. At the same time, Na-S and K-S batteries deliver theoretical energy densities of 1274[15] and 914 Wh kg^{-1},[16] respectively, which are far higher than the existing commercial batteries (**Figure 1B**). However, there are challenges in utilising the promising potential of Na-S and K-S batteries for their practical implementation. For instance, the high redox potential and the large size of Na^+ and K^+ can result in poor reaction kinetics, low operating voltage and severe volume change. In particular, the conversion reaction of S with Na^+ and K^+ ($Na^+/K^+/Li^+$: 1.09/1.38/0.76 Å) can cause a severe volume expansion of 171% and 309%, respectively, which is very much higher than the reaction with Li^+ (80%).[16,17] Also, the high redox potential of Na^+ and K^+ in relative to Li^+ (Na/K/Li: -2.7/-2.9/-3.0 V vs. standard hydrogen electrode (SHE)) lowers the cell voltage of Na-S and K-S batteries to 1.85 and 1.88 V, respectively. The two battery systems share the challenges that exist in the Li-S system, such as insulating nature of S, polysulphide shuttling and dendrite formation. In response, research on structural modification of S and its host matrix, new cell configuration, optimisation of binder and electrolytes, protection of the metal anode has seen a significant advancement in improving the electrochemical performance of Na-S and K-S batteries and gaining useful understanding of utilising carbon materials for the two types of batteries.

This review focuses on the role and effectiveness of carbon materials in addressing the challenges in Na-S and K-S batteries. We first discuss the fundamental electrochemistry of the batteries and then outline the critical challenges. Based on this, we discuss in detail the role of carbon materials in mitigating the challenges that different cell components, i.e., cathode, separator, and anode, are facing. Finally, we provide perspectives to highlight knowledge and technical gaps that need to be filled for the further development of Na-S and K-S batteries.

2. Electrochemistry of Na-S and K-S batteries

2.1. Phase transition of sodium sulphides

The typical configuration of a Na-S battery cell includes a Na metal anode and a S cathode, with a separator soaked in an organic electrolyte. Na-S batteries operate via a series of electrochemical conversion reactions between Na^+ and S. During discharge, Na-ions are electro-stripped from the Na metal anode, travel across the separator, and migrate to the S cathode. Electrons pass through the external circuit towards the S cathode. Therefore, S is reduced to form sodium disulphide (Na_2S) at the end of discharge. A reverse process occurs during charging to form S at the cathode and electroplate Na at the anode. They are expressed as below:

Anode: $Na \leftrightarrow Na^+ + e^-$ (1)

Cathode: $nS + 2Na^+ + 2e^- \leftrightarrow Na_2S_n\ (1 \leq n \leq 8)$ (2)

Among the 30 solid allotropes of S, cyclic orthorhombic S (α-sulphur, S_8) is the most thermodynamically stable allotrope at RT. The reduction of S_8 due to Na^+ intake causes ring opening of S_8, leading to the formation of chain length of various polysulphides.[18] In particular, the conversion reaction to form Na_2S does not occur in a single step but undergoes multistep reactions through the formation of different lengths of intermediate polysulphides.

The initial step of the conversion reaction begins with a solid-to-liquid transition due to the formation of high order polysulphides Na_2S_8 in a liquid state (Equation (3)). As discharge continues, Na_2S_8 is gradually reduced to Na_2S_4 (Equation (4)). The following conversion reaction of Na_2S_4 to form low order polysulphides Na_2S_3, Na_2S_2 and Na_2S is a liquid-to-solid state transition (Equation (5) and (6)). The final discharge product is generated from solid-solid transition from Na_2S_2 to Na_2S (Equation (7)).

$$S_8\,(s) + 2Na^+ + 2e^- \rightarrow Na_2S_8\,(l) \quad (3)$$

$$Na_2\,S_8(l) + 2Na^+ + 2e^- \rightarrow 2Na_2S_4(l) \quad (4)$$

$$Na_2S_4\,(l) + 2/3Na^+ + 2/3e^- \rightarrow 4/3Na_2S_3\,(s) \quad (5)$$

$$Na_2S_4(l) + 2Na^+ + 2e^- \rightarrow 2Na_2S_2(s) \quad (6)$$

$$Na_2S_2(s) + 2Na^+ + 2e^- \rightarrow 2Na_2S(s) \quad (7)$$

Among the various intermediate sodium polysulphides, the stable phases at RT are observed to be Na_2S_5, Na_2S_4, Na_2S_2 and Na_2S from the Na-S phase diagram **(Figure 2A).** [12]Based on the polysulphide species formed at various stages and the number of electrons transferred, specific capacity contribution from each of the polysulphide species is represented in **Figure 2B.**[19] The electrochemical potential at which the series of polysulphides are formed can be understood from the typical discharge profile of S_8 in Na-S batteries (**Figure 2C)**. The high voltage plateau region at 2.2 V corresponds to the solid-liquid transition between S_8 and Na_2S_8 and further reduction to Na_2S_4 lies in the sloping region from 2.2 V to 1.65 V. The reduction reaction between various insoluble polysulphides occurs in a low voltage region. The voltage plateau at 1.65 V represents the liquid-solid transition between Na_2S_4 and Na_2S_3/Na_2S_2. In the range of 1.65 to 1.2 V, final discharge product Na_2S is formed. It has been experimentally proven from in-situ synchrotron XRD studies that S_8 was reduced to Na_2S with the formation of Na_2S_x, Na_2S_4, Na_2S_2 as the intermediate polysulphides. The subsequent charge process involves the oxidation of Na_2S to form Na_2S_4 and Na_2S_x, without the formation of Na_2S_2. It has been

experimentally proven from in-situ synchrotron XRD studies that S_8 was reduced to Na_2S with the formation of intermediate polysulphides including Na_2S_x, Na_2S_4, and Na_2S_2. But the subsequent charge process involved the oxidation of Na_2S to form Na_2S_4 and Na_2S_x, without the formation of Na_2S_2. At the end of the charge process, S_8 was formed along with Na_2S_x, indicating the partial conversion reversibility between Na_2S and S_8 (Figure 2E). This reveals that reaction pathways can be distinct during charge and discharge processes. It is worth noting that the reduction pathway for the above conversion reaction between small S molecules (S_2-S_4) and Na^+ is distinct in comparison to S_8. The reduction of S_2-S_4 occurs through two steps (**Figure 2D**), Plateau I in the voltage profile above 1.4 V representing the formation of Na_2S_2 and Plateau II below 1.4 V representing the reduction of Na_2S_2 to Na_2S.

2.2 Phase transition of potassium sulphides

The cell configuration of K-S batteries is analogous to that of Na-S batteries, consisting of a K metal anode, a S cathode, and a separator in an organic electrolyte. The charge/discharge process involves reversible electroplating/electrostripping of K metal at the anode and oxidation/reduction reaction of S at the cathode. The electrochemical reduction pathway of S_8 in K-S batteries is similar to Na-S batteries with the formation of multiple intermediate potassium polysulphides.

$$S_8 \leftrightarrow K_2S_6 \leftrightarrow K_2S_5 \leftrightarrow K_2S_4 \leftrightarrow K_2S_2 \leftrightarrow K_2S \quad (8)$$

Liquid-state high order potassium polysulphides K_2S_n ($5 \leq n \leq 6$) and insoluble low order polysulphides K_2S_n ($1 \leq n \leq 4$) are formed during a discharge process. K-S phase diagram indicates that potassium polysulphides K_2S_n (n= 1, 2, 3, 4, 5, 6) are stable at room temperature (**Figure 3A)**. Based on the number of electrons transferred, theoretical specific capacities at various stages of polysulphide formation are represented in **Figure 3B.** The discharge/charge profiles of K-S batteries with S_8 as the cathode signals phase transformation from S_8 to end

discharge product K_2S. The sloping region between 2.25-1.65 V (Region I-II) corresponds to the reduction of S_8 to K_2S_6, and the plateau region from 1.6 to 1.2 V (Region III) corresponds to the conversion of K_2S_6 to K_2S_4 and K_2S_2. Formation of end discharge product K_2S occurs in the sloping region between 1.2 and 1 V (**Figures 3C and D**).

The reduction pathway and discharge/charge profiles for small S (S_2-S_4) as well as chemically bonded S differ from S_8, as reduction and oxidation reactions occur at a relatively lower potential compared to those of S_8 (**Figure 3E**). The strong chemical interaction between small S and carbon atoms results in charge delocalisation, which is responsible for lower voltage redox reactions compared to S_8/C cathodes.[23] The electrochemical reduction of elemental S in sulphurised polyacrylonitrile (SPAN) from 2 to 1 V (sloping region I-II) indicates the formation of K_2S_3 and K_2S_2. The process in following voltage range (1-0.3 V) signals the co-existence of K_2S_3, K_2S_2 and K_2S. Further discharge down to 0.1 V corresponds to the formation of K_2S along with K_2S_2 and K_2S_3 (**Figure 3F).** As K_2S_3 is more thermodynamically stable compared to K_2S (ΔG°_f = -528 kJ mol^{-1} vs. ΔG°_f = -410 kJ mol^{-1} for K_2S_3 and K_2S, respectively), K_2S_3 co-exists at the end of discharge.[24] In addition, a higher formation energy of K_2S_2 can results in its disproportionation reaction to form K_2S_3 and K_2S,[23] which often leads to sluggish reaction kinetics coupled with an incomplete reduction to form K_2S.[25]

Although Na-S and K-S batteries exhibit a similar process of S redox reaction pathway, there exist differences in the ion storage process due to the intrinsic properties of Na and K. The distinct feature in the discharge mechanism of Na-S and K-S batteries lies in the operational voltage of polysulphide formation and more specifically, the voltage range for the formation of low order polysulphides. The formation of K_2S occurs at a much lower voltage (1.2 to 1 V) compared to Na_2S (1.65 to 1.2 V). This is due to the fact that reaction energy ($\Delta_rG_m^\circ$) for the latter is more negative than the former (Na_2S = -323.249 kJ mol^{-1} vs. K_2S= -38.02 kJ mol^{-1}).[2627] Also, a lower lattice energy of K_2S (1979 kJ mol^{-1}) results in a lower voltage compared to the

lattice energy of Na_2S (2192 kJ mol^{-1}). Partial irreversibility during the charge process has been observed in both Na-S and K-S batteries. At the end of charge, Na_2S_x (x>2) co-exists with S due to the irreversible oxidation of discharged product Na_2S. In K-S batteries, partial oxidation of discharged products K_2S_3, K_2S_2, and K_2S results in the co-existence of K_2S_5 and K_2S_6 at a charged state.[28] The formation of K_2S during discharge significantly contributes to the irreversibility, as the lack of solution reaction pathway for the oxidation of K_2S causes the accumulation of K_2S, which acts as a "dead" polysulphide in the following cycles.[29]

3. Key challenges in Na-S and K-S batteries

Although S redox chemistry is promising in terms of reversible capacity and energy density, there are critical challenges associated with electrode materials and electrolytes, which imposes obstacles for the practical use of Na-S and K-S batteries, as the two battery systems share similar electrochemistry fundamentals and electrode/electrolyte design principles.

3.1 Insulating nature and volume expansion of S

The intrinsic insulating nature of S (~5.1×10^{-30} S cm^{-1}) deteriorates efficient transport of electrons within the cathode structure. This leads to low S utilisation, poor rate performance and high internal resistance in the cell. The accumulation of discharged products (Na_2S/K_2S) that are formed during electrochemical processes further builds up resistance in the cathode. For instance, elemental S used as the cathode in a Na-S battery delivered a specific capacity of 489 mAh g^{-1} in the initial cycle and exhibited a degradation in capacity in the subsequent cycles, stabilising at only 40 mAh g^{-1} after 20 cycles.[32,33] Although mechanical mixing of S with C can improve electronic conductivity to a limited extent, the weak binding of between S and C results in an inefficient electrical network within the cathode structure, which cannot largely increase cell capacity.[34] Volume expansion is a serious concern which severely affects

the durability of Na-S and K-S batteries. The volume change in Na-S and K-S batteries is more prominent than that in Li-S batteries due to the larger size of Na^+ and K^+ compared to Li^+. During the conversion process, the electrochemical reaction of S with Na^+/K^+ forms a series of high and low order polysulphides. As high order long-chain polysulphides are in a liquid state, they do not impose a huge volume change, but low order polysulphides are in a solid state; as a result, the density change that occurs during the conversion reaction of S_8 (1.96 g cm^{-3}) to a low order Na_2S (1.86 g cm^{-3}) leads to a volume change of ~260 %.[35] Similarly, formation of K_2S in K-S batteries induces a volume change of ~309%. The dramatic volume change causes the pulverisation of cathodes and the loss of their structural integrity. In a study carried out by Zhao et al., the diameter of porous carbon nanofibre/S (PCNF/S) changed from 180 to 240 nm during K^+ interaction with S. The expansion of PCNF/S led to a change in overall thickness of the cathode from 77 to 110 μm (**Figures 4A and 4B**).

3.2 Sluggish kinetics of Na_2S/K_2S

Theoretically, capacity generated from the conversion reaction between Na_2S_2/K_2S_2 and Na_2S/K_2S contributes to ~2/3 of the theoretical capacity of S. However, reaction kinetics of the $Na_2S_4 \leftrightarrow Na_2S$ and $K_2S_3 \leftrightarrow K_2S$ conversions is sluggish because it involves a liquid-solid reaction for the former and a solid-solid reaction for the latter. Moreover, K_2S_3 is more stable compared to K_2S in K-S batteries (ΔG°_f =-528 kJ mol^{-1} vs. ΔG°_f =-410 kJ mol^{-1} for K_2S_3 and K_2S), making the reaction more inclined to form K_2S_3 rather than K_2S.[36] For instance, K_2S_3 was detected as the final discharge product in a K-S battery using the S/mesoporous carbon cathode (**Figure 4C**). The incomplete reduction of S led to only 32% of theoretical capacity value.[36] Similar phenomena of low capacity due to slow transition kinetics of polysulphides has been observed in Na-S batteries,[37] where Na_2S_2 formed along with Na_2S after discharging the rGO/VO_2/S cathode to 0.5 V, delivering 52.3% of the theoretical capacity of S.[38]

3.3 Polysulphide shuttle effect and low material utilisation

The polysulphide shuttle effect is a major challenge in Na-S and K-S batteries, as it deteriorates cycle life and coulombic efficiency (CE) and promotes self-discharge. The effect is caused by the generation of long chain polysulphides that are highly soluble in organic solvents such as 1,2 dimethoxyethane (DME) and 1,3-dioxolane (DOL).[36] and the subsequent migration of the dissolved polysulphides towards Na/K anode and the reduction by the anode to form insoluble short chain polysulphide Na_xS_n/K_xS_n. As an example, a S/mesoporous carbon cathode of a K-S cell exhibited an initial discharge capacity of only ~51% of theoretical capacity and a charge capacity that was 11 times higher than the discharge capacity, resulting in a very low initial CE of ~8.1% (**Figure 4D**).[39] The dissolution of soluble polysulphides was also visually proven by the colour change of the electrolyte (**Figures 4E and 4F**). In another example, severe polysulphide shuttling occurred when S loading doubled the optimum loading in microporous carbon (~80 wt%)[40] and caused a low CE of ~80% and low S utilisation indicated by a capacity of <100 mAh g^{-1}. Furthermore, polysulphides that are reduced at the anode can diffuse back to the cathode and be re-oxidised, causing an issue of self-discharge. It has been observed in Na-S batteries that after cells rest for a period over 16 days, open circuit potential decreased and charge transfer resistance increased during cell operation.[39]

3.4 Unstable SEI and dendrite growth at anode

Na-S and K-S batteries use metal Na and K as the anode, respectively, and this increases safety risk. Because side reactions take place between the anode and electrolyte, a non-uniform SEI layer is formed, which allows for uneven electroplating of Na^+/K^+ at the anode and result in the formation of Na/K dendrites. The low mechanical stability of SEI layer and the volume change during electrodeposition can further cause cracks on the surface of the anode, which facilitates dendrite growth due to the enhanced ionic flux. Moreover, polysulphide species migrating

towards the anode deposit on the anode surface, increasing the internal resistance of the cell. As seen from a Na-S, pits and cracks gradually formed on the initially smooth surface of the Na anode during the discharge process, and the cracks were present even at the end of the charge process. In another study, needle-like structures of Na and non-uniform S deposits were found on the surface of the Na anode

The challenges discussed above can be closely related to a specific cell component in a Na-S or K-S battery. For instance, section 3.2 and 3.4 are related to the cathode and anode, respective, while section 3.3 can be dealt with by improving the separator. This review will address various the challenges via utilising carbon materials in the upcoming sections with the correlation to various cell components. Section 4 to 6 will highlight the role of carbon composite as a cathode. Section 7 will discuss the methods to control polysulphide shuttling and improve reaction kinetics using carbon composites at the separator. The section 8 will discuss using carbon materials to suppress dendrite formation at the Na/K anode and reinforce the mechanical stability of the anode.

4. Control volume expansion and improve reaction kinetics

4.1 Carbon as a conducting and buffering matrix for S_8 cathode

It is not ideal to directly use elemental S a cathode in Na-S and K-S batteries due to its insulating nature. Hence, S is always accompanied with an electrically conductive carbon. Besides acting as a conducting matrix, carbon plays multiple roles including a medium to buffer the volume change of S, a conducting host for discharged product(s), and a physical confinement for the dissolution of soluble polysulphides. These roles of carbon cannot be realised by a simple physical mixing of S with carbon, as it is not efficiently effective due to the weak interaction between carbon and S, resulting in poor electrochemical performance. As a result, infusing S into the pores of a carbon matrix provides a homogeneous distribution of S

within the matrix and strong interaction between carbon and S. To infuse S_8 inside a porous carbon matrix, S_8 is heated above its melting point, at which molten S_8 is impregnated into the pores by a capillary force and retains its cyclic molecular form. Among various porous carbon, micro and mesoporous carbon (> 1 nm) is preferable to accommodate 0.84 nm sized cyclo-S_8, as there is strong interaction and provision for a high loading of S_8.

For instance, the homogeneous distribution of 48 wt% S_8 in hollow mesoporous carbon spheres (HMCSs) delivered an initial capacity of 683 mAh g^{-1} at 0.1 C (**Figure 5A**).[42] Wang et al. designed similar hollow carbon spheres (IHCSs) with interconnected mesopores (**Figures 5B and 5C,**[43] which were suitable for a high S loading of 59 wt%. The conversion reaction of S_8 with Na^+ formed a final discharge product Na_2S_4, resulting in a reversible capacity of 391 mAh g^{-1} at 0.1 A g^{-1}. As the interconnected pores served as a medium to accommodate volume change, capacity retention of 85.6% was obtained after 100 cycles. The authors also highlighted the significance of IHCSs by comparing them with mesoporous carbon (MC) and reduced graphene oxide (rGO). Na-S cells using S_8/MC and S_8/rGO as cathodes delivered initial capacities of 285 and 200 mA h g^{-1} respectively. In the subsequent cycles, the cells failed to deliver a reversible capacity with a quick drop. This proved that IHCSs provided more sufficient sites for the discharge product and confine the soluble polysulphides more effectively than MC and rGO. Apart from porous carbon, a flexible carbon substrate can provide additional benefits for S_8 cathode, including high mechanical stability and the elimination of binder, current collector and conducting additive as the substrate is freestanding. Based on this approach, Chen's group prepared a flexible cathode for Na-S batteries using a carbon fibre cloth (CFC**) (Figure 5D)**.[44] The CFC formed a 3D interconnected network and S was loaded into the interconnected pores and on the surface of the CFC. With a S loading of 2 mg cm^{-2}, CFC/S delivered an initial capacity of 390 mAh g^{-1} at 0.1 C with a discharge product of Na_2S_2. Compared to S embedded in super P, CFC/S retained a much higher ~30% capacity after 300

cycles (~6.3% for C/S). As a proof of concept, a Na-S pouch-cell assembled using CFC/S cathode and Na anode delivered a capacity of 542 mAh g^{-1} at 0.05 C, and the cell showed negligible change in performance when powering LEDs at flat and bending states (**Figures 5E and 5F**). These results signified the mechanical stability of the cell, which was enabled by the CFC substrate. Flexible carbon matrix as a host for S has also been utilised in K-S batteries.[45] A freestanding CNT/S film delivered a capacity of 585 mAh g^{-1} at 50 mA g^{-1} and a stable cycling for 200 cycles.

Although there exists an interaction between carbon and S_8, the non-polar nature of a carbon matrix makes it less efficient to confine polar discharge products. The surface of carbon can be converted into a polar nature by doping heteroatoms such as N, S, and O, and at the same time, an increment in electrical conductivity of C/S composites can be obtained due to the promotion of electron donating properties.[46–48] Mou et al. prepared N-doped porous carbon nanosheets (NPCSs) as a conducting scaffold for S.[49] The rate performance of 42 wt% of S loaded in NPCSs exhibited a capacity of 280.9 mAh g^{-1} at 2 C in Na-S batteries. The presence of graphitic N in NPCSs acted as an electron donor site for S and hence delivered a capacity of 175 mAh g^{-1} at 2 C even when the S loading was increased to 55 wt%. With a very similar approach, Zhu's group doped 14.72 at% of graphitic N into porous carbon (NPC) derived from a metal organic framework.[50] With 50 wt% of S loading in NPC, S utilisation reached ~60% and a capacity of 220 mAh g^{-1} at 2 C was obtained. Besides N, S[51] and O[52] have been co-doped into carbon matrices to provide a strong confinement of S. The rapid electrochemical reaction kinetics due to N doping in porous carbon (PC) resulted in excellent rate performance of N,S co-doped PC/S (37 wt%) cathode in a Na-S cell, exhibiting 461 and 304 mAh g^{-1} at 2 and 10 C, respectively (**Figure 5G**). The strong chemical interaction between S and PC enabled stable cycling performance at 1 A g^{-1} with capacity retention of 90% after 500 cycles (**Figure 5H**). Confining S_8 in the porous carbon improved the rate performance of the cathode, but the

utilisation of S_8 was low (≤60%). It is worth considering that the low packing density of porous carbon can result in low volumetric energy density. Hence, it is necessary to explore various carbon nanostructures with optimal porosity to balance between S_8 loading and cell volumetric energy density. Confining S_8 in a doped carbon matrix can be explored further to obtain better S utilisation, compared to using pristine porous carbon.

4.2 Improving reaction kinetics using carbon composites

Poor reaction kinetics can arise by the liquid-solid and solid-solid transitions during the conversion reaction of S_8 with Na^+/K^+. The nucleation and deposition of discharged products onto the conducting carbon matrix results in poor transfer of electrons at the interface between conducting carbon and discharged products. This leads to an incomplete conversion of S_8 to Na_2S_4/Na_2S_2 instead of Na_2S. A strong binding of polysulphides towards the conducting matrix and subsequent rapid transfer of electrons are necessary for a complete conversion of soluble polysulphides to insoluble Na_2S/K_2S. As pristine carbon materials have a poor binding to polysulphides, Na_2S_2/Na_2S_4 will be formed as discharged products. Although heteroatom doped carbon develops a strong affinity to polysulphides, the poor catalytic activity can result in an incomplete reduction. This is due to the fact that a higher Gibbs free energy for the conversion of Na_2S_4 to Na_2S can cause sluggish kinetics and high polarisation (**Figure 6A**).[53] Hence, it is beneficial to have an electrocatalyst decorated in a carbon matrix for the efficient conversion reaction of S to yield final discharged products of Na_2S/K_2S. The most widely studied electrocatalyst so far is Co[26,53–56] due to its high catalytic activity and strong binding energy for polysulphides. By incorporating 15.7 wt% of Co nanoparticles (~10 nm) in S/porous carbon nanofibres (PCNF/S), the conversion reaction kinetics of sodium polysulphide has been enhanced,[53] as evidenced by an increase of Na^+ diffusion coefficient (D_{Na}) in the presence of the Co catalyst. As a result, the rate performance of Co-PCNF/S at 5 C was enhanced by 2.4

times compared to the PCNF/S cathode without the catalyst. The electrocatalytic activity of Co was also confirmed from a theoretical point of view. Enhanced electronic states near the Fermi energy level in Co-PCNF/S were responsible for the rapid transfer of electrons from Co to S, resulting in improved rate performance and a complete reduction to form Na_2S (**Figures 6B and 6C**). Moreover, the binding energies of sodium polysulphides on the surface of Co N-doped graphene (Co-NG) were more negative when compared to NG, which signified the adsorption capability of Co-PCNF/S enabling a long-term cycling of over 600 cycles. Similarly, N-doped Co is electrochemically active to accelerate the reaction kinetics of potassium polysulphides.[26] N-doped Co nanocrystals embedded in N-doped porous carbon (NPC) reduced the energy barrier for the conversion from high order to low order potassium polysulphides (**Figure 6D**). The authors increased the catalytic sites by reducing the nanocrystal size from 7 to 2 nm. The enhancement of the electrocatalytic activity of N-doped Co (2-3 nm) in NPC/S cathode can be seen from the high exchange current density in the Tafel plots (**Figure 6E**), where the cathodic and anodic exchange current densities of N-Co-NPC/S were increased by 4.2 and 2.4 times, respectively, compared to those of Co-NPC/S. Furthermore, a lower charge transfer resistance in N-Co-NPC/S cathode enabled a higher D_k, delivering a capacity of 415 mAh g^{-1} at 0.4 A g^{-1}. Apart from using expensive metal electrocatalysts, metal chalcogenides have also been proven suitable to accelerate polysulphide conversion reactions. Dou's group utilised FeS_2 as an electrocatalyst in a highly S loaded cathode (70 wt%).[57] The activation of S by FeS_2 resulted in 87.8% of S utilisation in the initial cycle. Also, compared to N-doped and undoped carbon, the higher binding energy and lower diffusion barrier for Na^+ on the surface of FeS_2 facilitated rapid electron transfer and improved rate performance (139 mAh g^{-1} at 5 A g^{-1}). The formation of final discharged product Na_2S was confirmed from in-situ SAED pattern.

Although catalytic activity assists S_8 to form end discharge product Na_2S/K_2S, the capacity obtained in the further cycles declined to < 900 mAh g^{-1}. It is because the incomplete oxidation of sodium/potassium polysulphides to S_8 causes the accumulation of intermediate discharge products, which limits the full potential of the electrocatalyst. This calls for the understanding of the kinetic limitations affecting the reversibility of the conversion process in the charged state, which might open new avenues to design bifunctional electrocatalysts that can promote the reversibility of both charge and discharge processes.

5. Controlling the shuttle effect: bypassing the formation of high order polysulphides

Sulfur S_8 transforms to liquid-state high order polysulphides Na_2Sn/K_2Sn ($4 \leq n \leq 8$) by intaking Na^+/K^+ before the formation of final solid discharge product Na_2S/K_2S, which is a major reason causing the shuttle effect. Forming Na_2S/K_2S through bypassing the formation of high order polysulphides can eliminate the dissolution of polysulphide species, but the formation of high order polysulphides is inevitable when using S_8 cathode. Instead of relying on the solid-liquid-solid transition that starts from S_8, a direct solid-solid transition (S_4 to S_2) can eradicate the shuttle effect. Short-chain S molecules and chemically bonded S (which exists in the form of S_2-S_3) undergo a reduction reaction between S_4^{2-}, S_2^{2-}, and Na^+/K^+ to form insoluble solid Na_2S/K_2S, bypassing high order polysulphides. Therefore, using short-chain S molecules not only limits the shuttle effect but also enhances the reversibility of the conversion reaction to store Na^+/K^+.

5.1 Carbon host for short-chain S molecules

Metastable chain-like S allotropes S_2, S_3, S_4 have been generally confined and stabilised in microporous carbon framework.[58] When cyclic ring-like S_8 is subjected to heat treatment above 159˚C, ring opening occurs to form polymeric S chains with a minimum viscosity. Further

heating to above 444.6˚C causes the dissociation of polymeric S chains into short-chain S_2-S_4.[18] Reversing back to RT results in the reformation of S_8. In order to stabilise S_4-S_2 molecules, microporous carbon was utilised to confine linear S_2-S_4 in pores (~0.5 nm) and restrict their transformation back to S_8 (**Figure 7A**). In addition, microporous carbon has the benefit of confining discharge products, as the size of Na_2S_2/Na_2S is very close to that of the micropores in the carbon (**Figure 7B**). The utilisation of S_2-S_4 has been found electrochemically active in Na-S and K-S for the reversible conversion reaction to form Na_2S and K_2S, respectively. Based on this approach, Pint's group infiltrated 50 wt% S_4 into carbon spheres containing micropores (S_4@CS) of size 0.5 nm (**Figure 7C**).[59] The authors confirmed the formation of S_4 from the absence of the characteristic Raman peak of S_8. Using S4@CS as the cathode of a Na-S cell, the discharge profile exhibited two redox peaks at 1.7 and 0.9 V, corresponding to the formation of Na_2S_2 and Na_2S. Due to the insoluble nature of them, the cell showed stable durability for 1500 cycles at 1 C. Under a low rate of 0.1 C, ~91% of theoretical capacity was obtained in the initial cycle, signalling the effectiveness in utilising S. Besides porous carbon, 1 D carbon with a coaxial cable structure that has an inner layer of CNT and an outer layer of microporous carbon (CNT@MPC) was also utilised as a cathode **Figure 7D**).[60] The inner core CNT provided good electrical conductivity and the outer layer confined and stabilised S_2-S_4 in the pores. CNT@MPC/S_2-S_4 with a ~40 wt% S loading underwent a dual step process to yield Na_2S that was accommodated within the CNT@MPC structure (**Figure 7E**). Na_2S_2 has a size close to that of the pores, so it was formed at a high potential (Plateau I). Further reaction with Na^+ resulted in the formation of Na_2S at a low potential (Plateau II) due to the excess energy required to overcome the steric hinderance (**Figure 7F**). CNT@MPC/S_2-S_4 delivered a specific capacity of 1148 mAh g^{-1} at 0.1 C and high-rate performance of 800 mAh g^{-1} at 2 C owing to the enhanced electrical conductivity derived from the presence of the inner layer of CNTs. In another study of microporous carbon/small S

molecules, the formation of Na_2S along with thiosulfate species was confirmed by the XPS results)[61] S_2-S_3 confined in the microporous carbon (MPC/S_2-S_3) for K-S batteries also underwent a dual step process to form K_2S at the end of discharge (**Figure 7G**).[62] The high electrochemical activity of S_2-S_3 with K^+ and the stabilisation of S_2-S_3 in the microporous carbon delivered a high specific capacity of 1198 mAh g^{-1} at 20 mA g^{-1} . The formation of insoluble products resulted in excellent durability with capacity loss of 0.18% per cycle and nearly 100% CE. Simulation results showed that the formation energy of K_2S_2 was higher than K_2S and K_2S_3, suggesting that K_2S_3 and K_2S were the most stable phases formed during the potassiation.

5.2 Covalent S/carbon composites

Similar to small S molecules, chemically bonded S does not generate soluble polysulphides during the reaction with Na^+/K^+. Sulphurised polyacrylonitrile (SPAN) cathode has a structure that contains chemically bonded S to conductive carbon backbone Heat treatment of S_8 with polyacrylonitrile (PAN) ($\geq$ 300˚C) results in the simultaneous release of H_2S by the dehydrogenation of PAN and the cyclisation of -CN groups to form a heterocyclic compound.[63,64] During this process, S is embedded in the heterocyclic compound and exists in the form of oligo(sulphides) and thioamide structures.[65] Hence, S that is covalently bonded to carbon backbone exists in the form of short S chains -C-S_x-C-(x = 2-3), thereby acting as electrochemically active sites. The S in SPAN exists in the form of small S molecular states, which prevents the formation of soluble polysulphides and forms Na_2S/K_2S. For instance, C-S bond in SPAN (31 wt% S) was directly reduced to Na_2S, leading to a high initial specific capacity of 1158 mAh g^{-1} and a good cyclability of 70% capacity retention after 500 cycles.[66] Similarly, SPAN (45.5 wt% S) in a K-S battery delivered a reversible specific capacity of 1050 mAh g^{-1} at 0.5 C along with a stable cycling for 100 cycles.[67] It is the cleavage of S-S and C-S

bonds in SPAN network during discharge and the re-dimerisation during charge that was responsible for the high reversible specific capacity (**Figure 8A**). However, the deliverance of specific capacity at high rates was poor in Na-S and K-S batteries due to the poor electrical conductivity of the carbon backbone in SPAN. This can be enhanced by doping Te,[68] Se[69] and I[70] in C-S backbone. I-doping in SPAN doubled its electrical conductivity (5.90×10^{-10} S cm^{-1} for I@SPAN and 3.07×10^{-10} S cm^{-1} for SPAN) and improved its ionic conductivity owing to the formation of NaI. As a result, I@SPAN (~42 wt% S) delivered excellent rate performance, where the capacities at 2 C were increased by 31% and 13% for the Na-S and K-S cells, respectively (**Figure 8B**). Another approach to obtain covalent bonding of C-S structure is in-situ solvothermal method .[71] The interaction between CS_2 and red P formed C-S composite and the formation of phosphorous sulphide facilitated the formation of sp^2 hybridised carbon. The covalent S uniformly distributed with C-S bonds both across the boundary and interior of the composites. The utilisation of S was optimised by controlling the operational potential of the Na-S cell. When operated in the range of 0.5 to 3 V, covalent S resulted in a specific capacity of 724 mAh g^{-1}, but it was doubled (1335 mAh g^{-1}) when the cell was first cycled in the range to 0.01-3 V for a few cycles, which can be ascribed to the activation of S present in the interior of C-S composites. The Na-S cell exhibited a stable cycling with 83.1% capacity retention and 100 % CE after 600 cycles. High S utilisation due to the interaction of Na^+ with interior S was confirmed by ex-situ XRD analysis (**Figures 8C and 8D**). In the first cycle, Na_2S peak was less intense at 0.5 V, but after the activation below 0.5 V, the interlayer expansion caused by the incomplete oxidation of sodium sulphide resulted in the feasible intercalation of Na^+ and formation of Na_2S at 0.5 V in the subsequent cycles. Kim's group combined the benefit of micropores and covalent bonding in a single cathode material for Na-S batteries,[72] by infiltrating 30 wt% covalently bonded small S molecules into a microporous polymer PIM-1(**Figure 8E**). The formation of Na_2S at the end of discharge process delivered a specific

capacity of 556 mAh g^{-1}, and a nearly 100% CE testified the effect of the covalent bonding in controlling the shuttle effect (**Figure 8F**). It is evident from various studies that in comparison to S_8, small S and covalently bonded S control the polysulphide shuttling and improve S utilisation without electrocatalysts. But the challenging aspect is to retain the performance at a high loading of S, and this requires further study on the structural modification of carbon matrices to accommodate more S without disrupting electrochemical performance.

6. High loading of S in carbon/polysulphide catholyte composites

Conventional cathodes of NSBs and KSBs utilise solid S (S_8/small S/covalent S) distributed in a carbon matrix. Inhomogeneous distribution of a high loading of solid S in the carbon matrix is always a major concern, as it causes weak interaction between Na^+/K^+ and S embedded inside the core structure. Also, there is a probability of S losing contact with carbon matrix over long cycles. Introducing liquid polysulphides as cathodes, i.e., polysulphide catholytes, can provide a high loading and homogeneous distribution of active S in carbon support and improve energy density due to the elimination of inactive binder in the cathode composition. But incorporating a high concentration of liquid-phase catholyte in a porous carbon matrix is challenging due to the volume limitation of the current collector used in the cell. Freestanding carbon matrices are effective in accommodating highly concentrated liquid-phase catholytes. The three-dimensional interlinked pathways and porous nature of a freestanding carbon matrix can facilitate the homogeneous distribution of S even at a high loading, simultaneously improving the utilisation of S and the electrical conductivity of the electrode. Yu et al. prepared polysulphide catholyte Na_2S_6 (1.5 M of S) from the mixture of sublime S and Na_2S in tetraethylene glycol dimethyl ether (TEGDME).[74] Freestanding multi-walled carbon nanotube (MWCNT) fabric was used as a supporting and conducting matrix for the Na_2S_6 catholyte (**Figure 9A**), and the loading of S reached 60 wt%. Discharging process took place via two

steps for the formation of the final discharged product Na_2S. MWCNT/Na_2S_6 outperformed conventional S/super P cathode by exhibiting ~71% increase in specific capacity (**Figure 9B**). This was an indicative of uniform distribution of S in the MWCNT fabric, resulting in better utilisation of active material. However, the capacity of MWCNT/Na_2S_6 declined over the cycles due to the dissolution of polysulphides during the transition from high order to low order polysulfides. The authors limited the discharge cut-off potential to 1.8 V in order to obtain a stable capacity, which restricted the degree of transitioning to low order polysulfides. To improve the durability of NSBs that use a catholyte, Kumar et al. infiltrated Na_2S_6 catholyte (1.5 M of S) in a freestanding carbon cloth decorated with MnO_2 (CC@MnO_2/Na_2S_6) via hydrothermal method (**Figure 9C**).[75] The carbon cloth facilitated the electrical conductivity of the composite and MnO_2 retained the soluble polysulfides during the discharge process. With a S loading of 1.7 mg cm^{-2}, CC@MnO_2/Na_2S_6 delivered a specific capacity of 938 mAh g^{-1} at 0.2 A g^{-1}, and 67% capacity was retained after 500 cycles. Furthermore, the presence of the carbon cloth assisted in attaining an impressive rate performance of 555 mAh g^{-1} at 2 A g^{-1}. It was confirmed that thiosulfate complexes ($S_2O_3^{2-}$) formed during the interaction between the catholyte and MnO_2, which improved binding the soluble sodium polysulphides to MnO_2 and thus the durability of the NSB (**Figure 9D**). In a very similar approach, catholytes using polysulfide intermediates 0.05 M K_2S_6 and K_2S_5 were utilised as cathodes in KSBs.[76] The catholytes were added to a three-dimensional (3D) conducting MWCNT network by drop-casting technique. The conversion of the catholytes to K_2S_3 as the final product resulted in a capacity of 400 mA h g^{-1} at 0.1 C (**Figure 9E**). Based on the results of the K metal anode cell, a K metal free KSB was also demonstrated using a potassiated hard carbon anode and the catholytes and delivered a reversible capacity of 235 mA h g^{-1} at 0.1 C (**Figure 9F**). The above studies demonstrate that using catholytes is a promising approach to increase S loading without compromising S utilisation, in comparison to solid S_8. But the durability of Na-S and K-S cells

using catholytes is not satisfactory because the shuttling effect can be potentially enhanced as active materials are essentially dissolving in catholytes. The interplay between catholyte concentration and electrochemical performance needs more attention before the use of catholytes can deliver maximum benefits for Na-S and K-S batteries.

7. Carbon as a defence layer to control polysulphide shuttling effect

Soluble polysulphides formed during discharge are concentrated near the cathode, and the separator could act as a physical barrier for the migration of soluble polysulphides towards the anode. However, the large pores and non-polar nature of conventional separators (e.g., Celgard and glass fibre) are not able to effectively restrict the migration of polar polysulphides. Functionalising a separator to make it polar and tuning its porosity by surface coating can impede polysulphide shuttling and thereby enhance S utilisation.[77] Apart from functionalising separators, an additional layer introduced between the cathode and separator can simultaneously trap polysulphides and improve the electrical conductivity of the cathode. Using conductive carbon or carbon composite materials to modify the surface of a separator or as a functional interlayer provides the benefits of physically blocking the migration of soluble polysulphide species, chemically adsorption of the species, enhancing electron transfer and Na^+/K^+ diffusion at the cathode, and facilitating the completion of conversion reaction.

Coating carbon materials such as carbon nanotubes,[78,79] carbon nanofibers,[80] reduced graphene oxide[81,82] on separators has been widely investigated in Li-S batteries. Specifically, one-dimensional (1D) structures are highly attractive due to their high electrical conductivity and self-weaving nature, which can offer additional mechanical support to the cathode. A layer of single-walled carbon nanotubes (SWCNTs) was deposited on the surface of Celgard separator facing towards the cathode using a vacuum filtration technique.[30] SWCNTs coating formed a 3D interconnected network and the nanometric interspaces (~100 nm) in the network facilitated

in trapping soluble polysulphides (**Figure 10A**); hence, the cyclic stability of the K-S cell retained a high specific capacity of 600 mAh g^{-1} after 50 cycles, whilst without the coating, the performance declined to 200 mAh g^{-1} (**Figure 10B**). Failure to block polysulphides using the uncoated separator led to more S depositing on the K anode. The electrically conducting nature of SWCNTs assisted in oxidation and reduction of polysulphides at the interface between the cathode and separator, leading to an enhancement in active material (S) utilisation. The enhancement of durability has also been seen in Na-S cells by implementing a similar approach of coating 30 µm thick carbon nanofibres (CNFs) over sodiated Nafion separator.[83] The trapping of soluble species within the Na_2S cathode by CNFs resulted in a stable CE (> 95%) for 100 cycles (**Figure 10C**). Besides surface coating on separators, inclusion of a freestanding carbon layer, such as films of CNT, CNF, carbon foam (CF), between cathode and separator can physically trap soluble polysulphides.[19] Furthermore, the non-polar polytetrafluoroethylene (PTFE) coated carbon cloth as an interlayer aided in anchoring polysulphides by forming chemical bonding between F present in PTFE and Na_2S_6.[84] The modification of separator/interlayer with non-polar carbon materials has a weak interaction between carbon and polysulphides, limiting the dissolution of polysulphides only to a certain extent, which is less effective for long cycles.[19] On the other hand, individual polar materials confine the dissolution of soluble species effectively, but S utilisation is reduced due to its low electrical conductivity. [85] Hence, a composite of a polar material and carbon is the most feasible route to simultaneously limit polysulphide dissolution and improve S utilisation. For instance, coating a mixture of Fe^{3+}/polyacrylamide nanospheres and graphene on a glass fibre separator (FPNs-G) provided integrated benefits of the adsorption of potassium polysulphides by Fe^{3+}/polyacrylamide nanospheres; electrical conductivity and mechanical stability was offered by graphene. This multifunctional nature of FPNs-G separator in a K-S cell delivered a specific capacity of 639 mAh g^{-1} and a capacity retention of 73.2% after 400 cycles. Moreover,

composites of carbon and metal chalcogenides further accelerate S reduction to form low order polysulphides, due to the strong interaction between metal atoms and polysulphides. Based on this approach, modification of a glass fibre separator using hollow carbon sphere/MoS_2 (HCS/MoS_2) composites led to the reversible conversion of S to Na_2S (**Figure 10D**),[86] resulting in a high specific capacity of 1309 mAh g^{-1} at 0.1 C in a Na-S cell. S utilisation increased to 78% with the use of the functionalised separator compared to pristine separator (37%) due to the complete conversion to Na_2S (**Figure 10F**). Also, the strong chemical interaction derived from the electron transfer from Na_2S_6 to Mo atoms held the soluble species in the cathode and increased the durability of the cell to 1000 cycles. In a similar way, Jiang's group demonstrated an effective utilisation of highly loaded S cathode (71.4 wt%) using double barrier coating of $MoSe_2$/N-doped hollow carbon spheres and graphene oxide ($MoSe_2$/NHCS/GO) for NSBs (**Figure 10E**).[87] The synergistic benefit of NHCS, GO and $MoSe_2$ realised a Na^+ diffusion coefficient (D_{Na}) that was two order of magnitude higher compared to the pristine glass fibre separator (3.45×10^{-12} vs. 1.38×10^{-14} cm^2 S^{-1}). Therefore, a faster reaction kinetics of polysulphide conversion resulted in high-rate performance of 530 mAh g^{-1} at 2 C for the functionalised separator, which was ~20 times higher than the pristine glass fibre separator. The authors demonstrated by the theoretical calculations that a negative adsorption energy of Na_2S_2 and Na_2S on $MoSe_2$ and N-doped carbon greatly contributed to the rapid reaction kinetics of soluble polysulphides (**Figure 10G**). Moreover, a lower diffusion barrier energy of Na_2S on $MoSe_2$ was shown to assist in a higher S utilisation.

8. Suppression of dendrites formation and mechanical stability using carbon materials

Na-S/K-S batteries can outperform LIBs in terms of energy density due to the use of Na/K metal as the anode and the high Na/K intake in S. The major demerits of using Na/K anode, which restrains the practical application of Na-S/K-S batteries, include (i) safety concern due

to Na/K dendrite formation as a result of non-uniformly reversible electroplating and unstable SEI layer; (ii) corrosion of Na/K anode due to its reaction with soluble polysulphides in an organic electrolyte; (iii) the difficulty in processing Na/K metal into films due to its low metallic bonding energy. To supress dendrite formation, widespread attention has been given to approaches such as optimising electrolyte by tuning SEI layer formation, replacing pristine metal with carbon, using alloy-based metals, and surface modification of Na/K anode. This section will discuss the utilisation of carbon to overcome the challenges of using Na/K metal anode from the following aspects: (i) carbon can act as a scaffold for Na/K metal to reduce local current density and establish a uniformly reversible electroplating process; (ii) carbon can alleviate mechanical deformation of Na/K metal; (iii) carbon can form composites with alloying metals.

Compared with surface modification of metal anode[88,89] and optimisation of electrolytes,[90,91] embedding Na/K in a host matrix[92] was found to be effective in suppressing Na/K dendrite formation. This kind of strategy was applied via impregnating K metal into a freestanding scaffold made of multi-walled carbon nanotubes (CNTs) and MXene (CNT@ MXene), (**Figure 11A**). The homogeneous distribution of CNTs into MXene provided sufficient pathways for electron transport, and the existence of interconnected voids ensured a dense K metal loading. This also realised the benefit of controlling the volume variation of the anode during an electroplating process. The CE of the CNT@MXene/K anode was ~93.1%, which was nearly 1.5 times higher than that of Cu and Al current collectors. A low resistance for the nucleation of K on CNT@MXene reduced local current density and regulated a homogeneous distribution of ionic flux, resulting in a smooth morphology of the anode after cycling. The authors concluded that the potassium-philic nature due to the N-dopants and Ti vacancies in MXene was responsible for the long-term reversibility of K electroplating (**Figure 11B**). Moreover, the CNT@MXene/K anode was efficient in eliminating self-discharge that was

caused by the shuttling effect. This was because the anode immersed in the electrolyte containing S/polyacrylonitrile (SPAN) showed no obvious colour change and polysulphide absorption peaks, both of which were observed when using a bare K metal anode (**Figure 11 C**). A K-S cell assembled using CNT@ MXene/K as the anode and SPAN as the cathode outperformed the cell that used a bare K metal anode in terms of specific capacity and durability. The former delivers a specific capacity of 436 mAh g^{-1} at 0.1 C (250 mAh g^{-1} for bare K metal) with the capacity retention of 69.4% after 500 cycles (40% after 300 cycles for bare K metal). Besides directly modifying a metal anode to reduce dendrite formation, using a Na or K alloy anode can have the same result. In this regard, elements such as Sn, Sb, Bi undergo an alloying reaction involving more than one mole of Na^+/K^+ per mole of alloy and hence can deliver a high gravimetric energy density.[93] These types of alloying materials are considered to be highly potential anodes for Na-S/K-S batteries. Hassoun's group used sodiated Sn/C as an anode for Na-S batteries,[94] where S loaded in hollow carbon spheres cathode delivered a reversible specific capacity of 550 mAh g^{-1} with an average discharge voltage of 1 V. Although this approach avoids the use of Na metal in the Na-S full-cell, the Sn/C anode needed to be pre-sodiated in a half-cell containing Na metal. To completely avoid the use of Na/K, solid S can be replaced with solid sodium sulphide/potassium sulphide (Na_2S/K_2S) as the cathode. This allows to use intercalation-type carbon as the anode and the cathode plays a dual role of Na^+/K^+ resource and active S. Micron sized Na_2S/C cathode and hard carbon anode were utilised to construct a Na-S cell,[95] and it delivered a specific capacity of 350 mAh g^{-1} at C/20 with the additive fluoroethylene carbonate (FEC) present in the electrolyte, which optimised the SEI layer formation on the hard carbon anode (**Figure 11D**). Using a very similar strategy, Yue et al. introduced $Na_{15}Sn_4$/C as an anode and a Na_3PS_4-Na_2S-carbon composite as a cathode[96] The obtained Na-S cell exhibited high electrochemical performance of 724 mAh g^{-1} at 50 mA g^{-1} (**Figure 11E**). It was shown that the size of Na_2S had a profound effect on

electrochemical performance, as nano-sized Na_2S exhibited a higher capacity of 438 mAh g^{-1} after 50 cycles compared to the poor cyclability of micron-sized Na_2S.

Apart from dendrite formation, the mechanical stability of Na/K metal is crucial to the practical implementation of NaS/K-S batteries at a large scale. Integrating Na/K metal with high tensile strength materials such as graphene can greatly influence the mechanical property of the metal. Wang et al. prepared a composite of reduced graphene oxide and Na metal (Na@ rGO),[97] with special interest in processing Na metal into different shapes that could have high tensile strength and hardness. By adding 4.5% rGO into Na, tensile strength was enhanced by five times with no significant deterioration in the electrochemical performance. Even under the compressive pressure of 250 psi, Na@rGO films were easy to separate without change in dimensions, signifying improved hardness due to the addition of rGO (**Figure 11F**). Moreover, Na@rGO anode was corrosion resistant to soluble S species, as evidenced by the clear solution of S/1,3-dioxolane (S/DOL) even after 96 h from the time of the immersion of the Na@rGO anode. The surface of the bare Na metal anode dipped in S/DOL solution showed uneven deposit due to the precipitation of low order polysulphides, but the Na@rGO anode was observed to have a smooth surface with very few S deposit (**Figure 11G**). As these techniques demonstrate the resistance of Na/K anode towards S corrosion, extending the approach in Na-S and K-S cells can effectively improve electrochemical performance in terms of specific capacity and durability. It is worth paying attention to the modification of Na/K anode and various cathodes, such as S_8 and small/covalent S, as well as how the modification is compatible with various electrolytes.

9. Summary and perspectives

This review provides a timely report on the research progress of Na-S and K-S batteries, with special attention given to role of carbon and carbon composites in addressing the challenges

that cell components face in Na-S and K-S cells. Reaction pathways and critical challenges that stand out as a blockade in achieving theoretical energy density of Na-S and K-S batteries are briefly discussed. Strategies based on the role of carbon and carbon composites in addressing these challenges at cathode, anode and separator are highlighted and analysed. Although significant advancement has been made in Na-S and K-S batteries, understanding on ambiguous reaction mechanisms and unsolved issues urges researchers to continue to work on various aspects to meet the energy demand.

(1) Enhancing the utilisation of S

With a nominal voltage of 3.6 V, commercial LIBs deliver energy density of 250 Wh kg^{-1}. Although theoretical energy densities of Na-S and K-S batteries are far higher than that of LIBs, a low operating voltage will affect their practical energy density. As Na-S and K-S batteries operate in 1.7-1.8 V and 1.3-1.8 V, respectively, it is crucial to take advantage of the high specific capacity of S to deliver high energy density. It can be realised only by maximising the utilisation of S, since the conversion from Na_2S_2/K_2S_2 to Na_2S/K_2S contributes to ~2/3 of the theoretical specific capacity. However, due to the poor reaction kinetics of the conversion reaction, S/carbon composites in Na-S and K-S batteries delivered specific capacities in the range of 400-900 mAh g^{-1}. [51,53,98–100] Hence, electrocatalysts along with S cathode have been employed to accelerate the conversion reaction. The most widely studied electrocatalyst for this purpose is Co, [26,101]which is a low earth abundance and facing potential supply risk. Focus should be shifted to electrocatalysts based on cost-effective elements and the acceleration of the reaction kinetics of conversion process during charge and discharge, in order to maximise S utilisation. Apart from electrocatalysts, redox mediators can assist in accelerating the redox kinetics and reducing the diffusion barrier for the transition between liquid-solid and solid-solid polysulphides.[102,103] Studies on introducing redox mediators in the electrolytes for Na-S

and K-S batteries can be implemented. This opens up an effective approach of utilising S without the use of expensive electrocatalysts at the cathode.

(2) Effect of electrolytes

Organic electrolytes such as ester and ether-based electrolytes are being utilised in Na-S and K-S batteries. The dissolution of soluble polysulphides into the electrolyte causes parasitic side reactions and increases irreversibility of the conversion process. The side reactions due to polysulphide shuttling is more pronounced at a potential above 2.4 V than below it in K-S battery.[36,104] This limits the upper cut-off voltage to 2.4 V, which in turn restricts the reversible phase transformation back to S_8. Also, the dissolution of polysulphides increases the viscosity of the electrolyte and ionic resistance. Hence, use of alternative electrolyte solvents such as ionic liquid and phosphate-based electrolytes, optimisation of electrolyte concentration, and addition of electrolyte additives to suppress the dissolution can be effective approaches. It is crucial to understanding the electrochemical behaviour of S cathodes such as S_8, S_2-S_4, and covalent S in different electrolytes and electrolyte wettability in different porous structured carbon, which can facilitate the functioning of the mentioned approaches. Additionally, dendrite formation at the anode side can be suppressed by using additives such as inorganic metal salts, as alkali metal ions such as Cs^+ and Rb^+ in the electrolyte can regulate metal ion deposition.[105] It is worth mentioning that ion selective polymer electrolytes can be utilised to control polysulphide shuttling and leakage of electrolyte.

(3) Full cell optimisation

The approach of using a non-metal anode in view of safety is essential to implement batteries at a large scale. Reported studies using sodiated hard carbon as the anode demonstrated a specific capacity of <400 mAh g^{-1} and durability for 10 cycles.[95] Conventionally, pre-sodiation

of hard carbon anode has been carried out using either electrochemical method or direct contact with pristine metal to form a stable SEI layer. These methods are simple to implement in a laboratory scale but not feasible for commercial application, as disassembling and further assembly of a full cell will complicate manufacturing processes. Pre-sodiation of anode by spray coating of sodium naphthalene solution followed up by a drying process was found to be a scalable approach.[106] This approach helps the formation of a stable SEI layer and the process can be tuned to control the level of pre-sodiation by controlling the amount of sodium solution. Similar approaches can be attempted for non-metal anodes of Na-S and K-S batteries, which reduces the complexity in a pre-sodiation process. Another approach to protect Na/K metal anode by using Na^+/K^+ conducting polymers or inorganic materials can also be implemented to enhance safety without compromising on capacity. Furthermore, optimisation of potential window and cathode/anode mass ratio in Na-S and K-S full cells can provide further advancements. Besides anode, there are benchmark values for the cathode and electrolyte that need to be considered during the fabrication. This includes areal S loading of > 5 mg cm^{-2},[107] S content of 65% in the composite,[11] low electrolyte/S ratio of <10 µL mg^{-1}.[108] Most of the reported studies have used S loading of <2 mg cm^{-2} and high electrolyte to S ratio in Na-S and K-S batteries.[39,53,67,70,109] This leads to an over-estimation of electrochemical performance. For instance, a Na-S coin cell that was fabricated using S encapsulated in a bimetallic sulphides cathode with a loading of 2 mg cm^{-2} delivered a high capacity of 768 mAh g^{-1} at 0.5 A g^{-1}. But when scaled up to a pouch cell with a S loading of 5 mg cm^{-2}, the cell delivered energy density which was far below the theoretical value (384 Wh kg^{-1} at 0.1 A g^{-1}).[110] Hence it is essential to focus on studying Na-S and K-S batteries using practical parameters to accelerate the advancement towards commercialisation.

(4) Self-discharge study

Self-discharge is an important practical issue that is often overlooked in Na-S and K-S batteries. Self-discharge rate in metal-S batteries is estimated to be >50 % capacity fade per month, which is severe due to the shuttling effect compared to commercial LIBs (<3% capacity fade per month).[111] The self-discharge phenomenon undergoes extreme capacity fade at static condition when S loading is >2mg cm^{-2}. Systematic self-discharge studies in Na-S and K-S batteries have not been carried out so far. Along with the analysis of electrochemical performance, other analyses are equally important for understanding self-discharge and should be carried out , including quantification of self-discharge using static electrochemical studies, open circuit voltage measurement, and electrochemical impedance spectroscopy (EIS)measurements over a long duration. These analyses can deliver the corelation between self-discharge rate and various factors such as concentration of polysulphide species, current collector, and anode corrosion rate.

(5) Advanced characterisation

Sublimation rate of S under high vacuum condition is ~1 monolayer of S atoms per second, which makes it challenging to directly image of S/C nanocomposites using conventional SEM/TEM. Adopting cryogenic TEM to image S/C nanocomposites prevents the sublimation of S and provides accurate information on the distribution of S. Despite a large number of studies on nanostructured carbon hosts to confine the volume expansion of S, the extent of the control and its corelation to the carbon nanostructures are poorly understood. Also, rearrangement and distribution of S in the carbon host after each charge/discharge cycle vary, which further affects the S utilisation in the subsequent cycles. Although in-situ TEM provides morphological evolution of S, 1D or 2D images provide limited information on the morphological and volume change over the entire thickness of electrode. 3D imaging using X-ray computed tomography (X-ray CT) has the benefit of visualising the structural change of S

cathode at micro- and nano-scale and the distribution of S over the entire electrode thickness. Information gained from this kind of study helps to effectively design highly loaded S cathodes with the efficient utilisation of S. Furthermore, the non-destructive nature of cryo-STEM and X-ray CT finds its scope in analysing the electrodes of pouch/prismatic/cylindrical Na-S/K-S cells. The integrated techniques of cryo-STEM and X-ray CT for the study of SEI layer and dendrite formation will provide insights on the relationship between the shuttle effect and dendrite formation.

Despite the continued research interest and considerable improvement that has been achieved in Na-S and K-S batteries, the practical realisation of these batteries is still a long way to go. Most of the current research on Na-S and K-S is concentrated on cathode, with a particular focus of reducing shuttling effect. As advancement in one component (cathode) of a Na-S/K-S cell will not meet all the challenges, advancement in other components of the cell, including electrolyte, binder, and anode, needs to proceed at a same pace with cathode. Apart from the implementation of the strategies discussed in this review, demonstrating coin-cell performance with practical parameters can facilitate the translation of the battery technologies to a larger scale. Specifically, safety is a major concern when using a commercialised battery, particularly with highly reactive metal being present in the battery, in any kind of application. But ground research work is very limited on flame retardant materials and techniques to quantify safety on a laboratory scale, which is crucial to identify practical viability. Furthermore, experimental studies of Na-S and K-S battery operation at a low temperature are urgently needed to establish the operational temperature limit of the batteries, as large-scale energy storage is likely to occur in outdoor space where temperature variation can be significant. Finally, sustainable methods for recycling Na-S and K-S batteries at end-of-life require attention to reduce environmental impact and energy consumption. A combined advancement at the levels of cell materials and practical use will fast forward developing high energy density Na-S and K-S batteries.

Acknowledgments

The authors acknowledge the financial support from the Engineering and Physical Sciences Research Council (EP/V000152/1), the Leverhulme Trust (RPG-2021-138), and the Royal Society (RGS\R2\212324).

Author contributions

Conceptualisation, Y.X. and A.P.V.S.; Writing – Original Draft, A.P.V.S.; Writing – Review & Editing, Y.X. and A.P.V.S.; Supervision and Funding Acquisition, Y.X.

Declaration of interests

The authors declare no competing interests.

References

1. Moore, J., and Henbest, S. (2020). New Energy Outlook 2020. *BloombergNEF*, pp. 1-29.
2. Hesse, HC., Schimpe, M., Kucevic, D., Jossen, A., (2017). Lithium-ion battery storage for the grid - A review of stationary battery storage system design tailored for applications in modern power grids. *Energies*. 10 (12), 1-42.
3. Ralon, P., Taylor, M., Ilas, A., Diaz-Bone, H., and Kairies, K. (2017). Electricity storage and renewables: Costs and markets to 2030. *International Renew Energy Agency*. pp. 1-132.
4. Chen, H., Cong, TN., Yang, W., Tan, C., Li, .Y, Ding, Y. (2009). Progress in electrical energy storage system: A critical review. *Prog. Nat Sci*. 19 (3), 291-312.
5. Kravchyk, K V., Bhauriyal, P., Piveteau, L., Guntlin, CP., Pathak, B., Kovalenko, M V. (2018). High-energy-density dual-ion battery for stationary storage of electricity using

concentrated potassium fluorosulfonylimide. *Nat. Commun*. 9, 4469-4478.

6. Schmidt, O., Hawkes, A., Gambhir, A., Staffell, I. (2017). The future cost of electrical energy storage based on experience rates. *Nat. Energy*. 2, 17110.
7. Kim, DK., Yoneoka, S., Banatwala, AZ., Kim, Y-T., Nam, K-Y. (2018). Handbook on Battery Energy Storage System. *Asian Dev. Bank.* pp. 1-92.
8. May, GJ., Davidson, A., Monahov, B. (2018). Lead batteries for utility energy storage: A review. *J. Energy Storage*. 15, 145-157.
9. Zuo, Y., Liu, R., Zhang, X., Nadimicherla, R., Huang, J., Lu, Y., and Fu, R. (2019). A new supramolecular binder strongly enhancing the electrochemistry performance for lithium-sulfur batteries. *Chem. Commun*. 55 (92), 13924-13927.
10. Nikiforidis, G., Van de Sanden, MCM., Tsampas, MN. (2019). High and intermediate temperature sodium-sulfur batteries for energy storage: development, challenges and perspectives. *RSC Adv*. 9 (10), 5649-5673.
11. Manthiram, A., Fu, Y., Chung, S., Zu, C., Su, Y. (2014). Rechargeable Lithium − Sulfur Batteries. *Chem. Rev*. 114, 11751-11787.
12. Wang, .Y, Zhou, D., Palomares, V., Shanmukaraj, D., Sun, B., Tang, X., and Wang, G. (2020). Revitalising sodium-sulfur batteries for non-high-temperature operation: A crucial review. *Energy Environ. Sci*. 13 (11), 3848-3879.
13. Ding, J., Zhang, H., Fan, W., Zhong, C., Hu, W., Mitlin, D. (2020). Review of Emerging Potassium–Sulfur Batteries. *Adv. Mater*. 32 (23), 1908007.
14. Wang, P., Buchmeiser, MR. (2019). Rechargeable Magnesium–Sulfur Battery Technology: State of the Art and Key Challenges. *Adv. Funct. Mater*. 29, 1905248.
15. Eng, AYS., Kumar, V., Zhang, Y., Luo, J., Wang, W., Sun, Y., and She, Z.W. (2021). Room-Temperature Sodium–Sulfur Batteries and Beyond: Realizing Practical High Energy Systems through Anode, Cathode, and Electrolyte Engineering. *Adv. Energy*

Mater. 11 (14), 2003493.

16. Zhao, X., Lu, Y., Qian, Z., Wang, R., Guo, Z. (2020). Potassium- sulfur batteries: Status and perspectives. *EcoMat* 2 (3), e12038.
17. Gu, X.X., Yang, Z.G., Qiao, S., Shao, C Bin, Ren, X.L., Yang, J.J. (2021) Exploiting methylated amino resin as a multifunctional binder for high-performance lithium–sulfur batteries. *Rare Met*. 40 (3), 529-536.
18. Fang, R., Xu, J., Wang, D.W. (2020). Covalent fixing of sulfur in metal-sulfur batteries. *Energy Environ. Sci*. 13 (2), 432-471.
19. Yu, X., Manthiram, A. (2014). Capacity Enhancement and Discharge Mechanisms of Room-Temperature Sodium-Sulfur Batteries. *ChemElectroChem* 1 (8), 1275-1280.
20. Nikiforidis, G., Jongerden, G.J., Jongerden, E.F., van de Sanden, MCM, Tsampas, M.N. (2019). An Electrochemical Study on the Cathode of the Intermediate Temperature Tubular Sodium-Sulfur (NaS) Battery. *J Electrochem. Soc*. 166 (2), A135-A142.
21. Xin, S., Yin, Y.X., Guo, Y.G., Wan, L.J. (2014). A high-energy room-temperature sodium-sulfur battery. *Adv. Mater*. 26 (8), 1261-1265.
22. Zhang, B., Sheng, T., Liu, Y.D.,Wang, Y.X., Zhang, L., Lai, W.H., and Dou, S.X. (2018). Atomic cobalt as an efficient electrocatalyst in sulfur cathodes for superior room-temperature sodium-sulfur batteries. *Nat. Commun*. 9, 4082-4093.
23. Xiong, P., Han, X., Zhao, X., Bai, P., Liu, Y., Sun, J., and Xu, Y. (2019). Room-Temperature Potassium−Sulfur Batteries Enabled by Microporous Carbon Stabilized Small-Molecule Sulfur Cathodes. *ACS Nano*. 13, 2536-2543.
24. Yuan, X., Zhu, B., Feng, J, Wang, C., Cai, X., Qiao, K., and Qin, R. (2020). Electrochemical Insights, Developing Strategies, and Perspectives toward Advanced Potassium–Sulfur Batteries. *Small*. 16 (42), 1-25.
25. Lai, N.C., Cong, G., Lu, Y.C. (2019). A high-energy potassium-sulfur battery enabled

by facile and effective imidazole-solvated copper catalysts. *J. Mater. Chem. A*. 7 (36), 20584-20589.

26. Ge, X., Di, H., Wang, P., Miao, X., Zhang , P., Wang, H., and Yin, L. (2020). Metal-organic framework-derived nitrogen-doped cobalt nanocluster inlaid porous carbon as high-efficiency catalyst for advanced potassium-sulfur batteries. *ACS Nano*. 14 (11), 16022-16035.

27. Wenzel, S., Metelmann, H., Raiß, C., Katharina, A., Janek, J., Adelhelm, P. (2013). Thermodynamics and cell chemistry of room temperature sodium / sulfur cells with liquid and liquid / solid electrolyte. *J. Power Sources*. 243, 758-765.

28. Ma, R., Fan, L., Wang, J., Lu, B. (2019). Confined and covalent sulfur for stable room temperature potassium-sulfur battery. *Electrochim. Acta*. 293, 191-198.

29. Gu, S., Xiao, N., Wu, F., Bai, Y., Wu, C., Wu, Y. (2018). Chemical Synthesis of K_2S_2 and K_2S_3 for Probing Electrochemical Mechanisms in K-S Batteries. *ACS Energy Lett*. 3 (12), 2858-2864.

30. Yu, X., Manthiram, A. (2018). A reversible nonaqueous room-temperature potassium-sulfur chemistry for electrochemical energy storage. *Energy Storage Mater*. 15, 368-373.

31. Hwang, J.Y., Kim, H.M., Sun, Y.K. (2018). High performance potassium-sulfur batteries based on a sulfurized polyacrylonitrile cathode and polyacrylic acid binder. *J. Mater. Chem. A*. 6 (30), 14587-14593.

32. Park, C.W., Ahn, J.H., Ryu, H.S., Kim, K.W., Ahn, H.J. (2006). Room-Temperature Solid-State Sodium⁄Sulfur Battery. *Electrochem. Solid-State Lett*. 9 (3), A123.

33. Ryu, H., Kim, T., Kim, K., Ahn, J.H., Nam, T., Wang, G., and Ahn, H.J. (2011). Discharge reaction mechanism of room-temperature sodium-sulfur battery with tetra ethylene glycol dimethyl ether liquid electrolyte. *J. Power Sources*. 196 (11), 5186-

5190.

34. Xie, Y., Yin, J., Zheng, J., Wang, L., Wu, J., Dresselhaus, M., and Zhnag, X. (2019). Synergistic Cobalt Sulfide/Eggshell Membrane Carbon Electrode. *ACS Appl. Mater. Interfaces*. 11 (35), 32244-32250.

35. Manthiram, A., Yu, X. 2015. Ambient temperature sodium-sulfur batteries. *Small*. 11 (18), 2108-2114.

36. Zhao, Q., Hu, Y., Zhang, K., Chen J. (2014). Potassium−Sulfur Batteries A New Member of Room Temperature Rechargeable Metal-Sulfur Batteries. *Inorg. Chem*. 53, 9000-9005.

37. Yu, X., Manthiram, A. (2014). Highly Reversible Room-Temperature Sulfur/Long-Chain Sodium Polysul fi de Batteries. *J. Phys. Chem. Lett*. 5, 1943-1947.

38. Du, W., Wu, Y., Yang, T, Guo, B., Liu, D., Bao, S.J., and Xu, M. (2020). Rational construction of rGO/VO_2 nanoflowers as sulfur multifunctional hosts for room temperature Na-S batteries. *Chem. Eng. J*. 379, 122359.

39. Wang, L., Bao, J., Liu, Q., Sun, C. (2019). Concentrated electrolytes unlock the full energy potential of potassium- sulfur battery chemistry. *Energy Storage Mater*. 18, 470-475.

40. Guo, Q., Li, S., Liu, X, Chang, X., Zhang, H., and Xia, H. (2020). Ultrastable Sodium–Sulfur Batteries without Polysulfides Formation Using Slit Ultramicropore Carbon Carrier. *Adv. Sci*. 7 (11), 1903246.

41. Zhao, X., Hong, Y., Cheng, M., Wang, S., Zheng, L., Wang, J., and Xu, J. (2020). High performance potassium-sulfur batteries and their reaction mechanism. *J. Mater. Chem. A*. 8 (21), 10875-10884.

42. Du, W., Xu, Q., Zhan, R., Zhang, Y., Luo, Y., Xu, M. (2018). Synthesis of hollow porous carbon microspheres and their application to room-temperature Na-S batteries. *Mater.*

Lett. 221, 66-69.

43. Wang, Y.X., Yang, J., Lai, W.,Chou, S.L., Gu, Q.F., Liu, H.K. and Dou, S.X. (2016). Achieving High-Performance Room-Temperature Sodium−Sulfur Batteries with S@Interconnected mesoporous carbon hollow nanospheres. *J. Am. Chem. Soc*. 138, 16576-16579.

44. Lu, Q., Wang, X., Cao, J., Chen, C., Chen, K., Zhao, Z., and Chen, J. (2017). Freestanding carbon fiber cloth/sulfur composites for flexible room-temperature sodium-sulfur batteries. *Energy Storage Mater*. 8, 77-84.

45. Yuan, X., Zhu, B., Feng, J., Wang, C., Cai, X., Qin, R. (2021). High-Performance Stable Potassium–Sulfur Batteries Enabled by Free-Standing CNT Film-Based Composite Cathodes. *J. Electron. Mater*. 50 (6), 3037-3042.

46. Feng, X., Bai, Y., Liu, M., Li, Y., Yang, H., Wang, X., and Wu, C. (2021). Untangling the respective effects of heteroatom-doped carbon materials in batteries, supercapacitors and the ORR to design high performance materials. *Energy Environ. Sci*. 14 (4), 2036-2089.

47. Han, X.R., Guo, X.T., Xu, M.J., Pang, H., Ma, Y.W. (2020). Clean utilization of palm kernel shell: sustainable and naturally heteroatom-doped porous activated carbon for lithium–sulfur batteries. *Rare Met*. 39 (9), 1099-1106.

48. Zheng, B., Lin, X., Zhang, X., Wu, D., Matyjaszewski, K. (2020). Emerging Functional Porous Polymeric and Carbonaceous Materials for Environmental Treatment and Energy Storage. *Adv. Funct. Mater*. 30 (41), 1907006.

49. Mou, J., Liu, T., Li, Y., Zhang, W., Li, M., Xu, Y., and Liu, M. (2020). Hierarchical porous carbon sheets for high-performance room temperature sodium-sulfur batteries: Integration of nitrogen-self-doping and space confinement. *J. Mater. Chem. A*. 8 (46), 24590-24597.

50. Chen, Y.M., Liang, W., Li S, Zou, F., Bhaway, S.M., Qiang, Z., and Zhu, Y. (2016). A nitrogen doped carbonized metal-organic framework for high stability room temperature sodium-sulfur batteries. *J. Mater. Chem. A.* 4 (32), 12471-12478.

51. Xiao F, Yang X, Wang H, Xu, J., Liu, Y., Yu, D.Y., and Rogach, A.L. (2020). Covalent Encapsulation of Sulfur in a MOF-Derived S, N-Doped Porous Carbon Host Realized via the Vapor-Infiltration Method Results in Enhanced Sodium–Sulfur Battery Performance. *Adv. Energy Mater*. 10 (23), 2000931.

52. Xia, G., Zhang, L., Chen X, Hunag, Y., Sun, D., Fang, F., and Yu, X. (2018). Carbon hollow nanobubbles on porous carbon nanofibers: An ideal host for high-performance sodium-sulfur batteries and hydrogen storage. *Energy Storage Mater*. 14, 314-323.

53. Yang, H., Zhou, S., Zhang, B.W., Chu, S.Q., Guo, H., Gu, Q.F., and Dou, S.X. (2021). Architecting Freestanding Sulfur Cathodes for Superior Room-Temperature Na–S Batteries. *Adv. Funct. Mater*. 31 (32), 2102280.

54. Du, W., Gao, W., Yang, T., Guo, B., Zhang, L., Bao, S.J., and Xu, M. (2020). Cobalt nanoparticles embedded into free-standing carbon nanofibers as catalyst for room-temperature sodium-sulfur batteries. *J. Colld. Inter. Sci*. 565, 63-69.

55. Zhang, B.W., Sheng, T., Liu, Y.D., Wang, Y.X., Zhang, L., Lai, W.H. and Dou, S.X. (2018). Atomic cobalt as an efficient electrocatalyst in sulfur cathodes for superior room-temperature sodium-sulfur batteries. *Nat. Commun*. 9, 4082.

56. Du, W., Shen, K., Qi, Y., Gao, W., Tao, M., Du, G., and Xu, M. (2021). Efficient Catalytic Conversion of Polysulfides by Biomimetic Design of "Branch-Leaf" Electrode for High-Energy Sodium–Sulfur Batteries. *Nano-Micro Lett*. 13, 50.

57. Yan, Z., Liang, Y., Xiao, J., Lai, W., Wang, W., Xia, Q. and Dou, S.X. (2020). A High-Kinetics Sulfur Cathode with a Highly Efficient Mechanism for Superior Room-Temperature Na–S Batteries. *Adv. Mater*. 32 (8), 1906700.

58. Xin, S., Gu, L., Zhao, N.H., Yin, Y.X., Zhou, L.J., Guo, Y.G., and Wan L.J. (2012). Smaller sulfur molecules promise better lithium'sulfur batteries. *J. Am. Chem. Soc*. 134 (45), 18510-18513.

59. Carter, R., Oakes, L., Douglas, A., Muralidharan N., Cohn A.P., Pint, C.L. (2017). A Sugar-Derived Room-Temperature Sodium Sulfur Battery with Lon,g Term Cycling Stability. *Nano. Lett*. 17, 1863-1869.

60. Xin, S., Yin, Y., Guo, Y., Wan, L. (2014). A High-Energy Room-Temperature Sodium-Sulfur Battery. *Adv. Mater*. 26, 1261-1265.

61. Wei, S., Xu, S., Agrawral, A., Choudhury, S., Lu, Y., Tu, Z. and Archer, L.A. (2016). A stable room-temperature sodium–sulfur battery. *Nat. Commun*. 7, 11722.

62. Xiong P, Han X, Zhao X, Bai, P., Liu, Y., Sun, J., and Xu, J.(2019). Room-Temperature Potassium − Sulfur Batteries Enabled by Microporous Carbon Stabilized Small-Molecule Sulfur Cathodes. *ACS Nano*. 13, 2536-2543.

63. Wang, J., He, Y.S., Yang, J. (2015). Sulfur-based composite cathode materials for high-energy rechargeable lithium batteries. *Adv. Mater*. 27 (3), 569-575.

64. Wei, S., Ma, L., Hendrickson, K.E., Tu, Z., Archer, L.A. (2015). Metal−Sulfur Battery Cathodes Based on PAN−Sulfur Composites. *J Am Chem Soc*. 137, 12143-12152.

65. Fanous, J., Wegner, M., Grimminger, J., Andresen, Ä., Buchmeiser, M.R. (2011). Structure-related electrochemistry of sulfur-poly(acrylonitrile) composite cathode materials for rechargeable lithium batteries. *Chem. Mater*. 23 (22), 5024-5028.

66. Tae, H.H., Dae, S.J., Joo-Seong, K., Byung, G.K. and JWC. (2013). One-Dimensional Carbon−Sulfur Composite Fibers for Na−S Rechargeable Batteries Operating at room temperature. *Nano Lett*.13, 4532-4538.

67. Hwang, J.Y., Kim, H.M., Sun, Y.K. (2018). High performance potassium-sulfur batteries based on a sulfurized polyacrylonitrile cathode and polyacrylic acid binder. *J.*

Mater. Chem. A. 6 (30), 14587-14593.

68. Li, S., Zeng, Z., Yang, J., Han, Z., Hu, W., Wang, L., and Xie, J. (2019). High Performance Room Temperature Sodium−Sulfur Battery by Eutectic Acceleration in Tellurium doped sulfurized Polyacrylonitrile. *ACS Appl. Energy Mater*. 2, 2956-2964.

69. Chen, X., Peng, L., Wang, L., Yang, J., Hao, Z., Xiang, J., and Xie, J. (2019). Ether-compatible sulfurized polyacrylonitrile cathode with excellent performance enabled by fast kinetics via selenium doping. *Nat. Commun*. 10, 1021.

70. Ma, S., Zuo, P., Zhang, H., Yu, Z., Cui, C., He, M., and Yin, G. (2019). Iodine-doped sulfurized polyacrylonitrile with enhanced electrochemical performance for room-temperature sodium/potassium sulfur batteries. *Chem. Commun*. 55 (36), 5267-5270.

71. Yan, J., Li, W., Wang, R., Feng, P., Jiang, M., Han, J., and Jiang, K. (2020). An in Situ Prepared Covalent Sulfur − Carbon. *ACS Energy Lett*. 5, 1307−1315.

72. Jeon, J. W., Kim, D. M., Lee, J., Lee, J. C., Kim, Y. S., Lee, K. T., & Kim, B. G. (2020). PIM-1-based carbon-sulfur composites for sodium-sulfur batteries that operate without the shuttle effect. *J. Mater. Chem. A*. 8 (7), 3580-3585.

73. Yan, J., Li, W., Wang, R., Feng, P., Jiang, M., Han, J., and Jiang, K. (2020). An in Situ Prepared Covalent Sulfur−Carboncomposite electrode for high performance room temperature sodium sulfur batteries. *ACS Energy Lett*. 5, 1307-1315.

74. Yu, X., and Manthiram, A. (2014). Room-temperature sodium-sulfur batteries with liquid-phase sodium polysulfide catholytes and binder-free multiwall carbon nanotube fabric electrodes. *J. Phys. Chem. C*. 118 (40), 22952-22959.

75. Kumar, A., Ghosh, A., Roy, A., Panda, M. R., Forsyth, M., MacFarlane, D. R., and Mitra, S. (2019). High-energy density room temperature sodium-sulfur battery enabled by sodium polysulfide catholyte and carbon cloth current collector decorated with MnO_2 nanoarrays. *Energy Storage Mater*. 20, 196-202.

76. Hwang, J. Y., Kim, H. M., Yoon, C. S., & Sun, Y. K. (2018). Toward High-Safety Potassium−Sulfur Batterues using a potassium polysulfide catholyte and Metal-free anode. *ACS Energy Lett*. 3, 540-541.

77. Lin, X., Liang, Y., Lu, Z., Lou, H., Zhang, X., Liu, S., and Wu, D. (2017). Mechanochemistry: A Green, Activation-Free and Top-Down Strategy to High-Surface-Area Carbon Materials. *ACS Sustain. Chem. Eng*. 5 (10), 8535-8540.

78. Liu, B., Wu, X., Wang, S., Tang, Z., Yang, Q., Hu, G. H., & Xiong, C. (2017). Flexible carbon nanotube modified separator for high-performance lithium-sulfur batteries. *Nanomaterials*. 7 (8), 196.

79. He, J., Gao, Z., & Li, X. (2021). Yeast-Derived Carbon Nanotube-Coated Separator for High Performance Lithium-Sulfur Batteries. *JOM*. 73 (8), 2516-2524.

80. Guan, Y., Liu, X., Akhtar, N., Wang, A., Wang, W., Zhang, H., Suntivich, J. and Huang, Y., (2019). Cr_2O_3 Nanoparticle Decorated Carbon Nanofibers Derived from Solid Leather Wastes for High Performance Lithium-Sulfur Battery Separator Coating. *J. Electrochem. Soc*. 166 (8), A1671-A1676.

81. Zhang, Y., Miao, L., Ning, J., Xiao, Z., Hao, L., Wang, B. and Zhi, L. (2015). A graphene-oxide-based thin coating on the separator: An efficient barrier towards high-stable lithium-sulfur batteries. *2D Mater*. 2 (2), 024013.

82. Lin, W., Chen, Y., Li, P., He, J., Zhao, Y., Wang, Z., Liu, J., Qi, F., Zheng, B., Zhou, J. and Xu, C. (2015). Enhanced Performance of Lithium Sulfur Battery with a Reduced Graphene Oxide Coating Separator. *J. Electrochem. Soc*. 162 (8), A1624-A1629.

83. Yu, X. and Manthiram, A. (2016). Performance Enhancement and Mechanistic Studies of Room-Temperature Sodium-Sulfur Batteries with a Carbon-Coated Functional Nafion Separator and a Na_2S/Activated Carbon Nanofiber Cathode. *Chem. Mater*. 28 (3), 896-905.

84. Vijaya Kumar Saroja AP, Muthusamy K, Sundara R. (2019). Strong Surface Bonding of Polysulfides by Teflonized Carbon Matrix for Enhanced Performance in Room Temperature Sodium-Sulfur Battery. *Adv. Mater. Interfaces*. 6 (7), 1801873.

85. Meyerson, M.L., Papa, P.E., Weeks, J.A., Paul-Orecchio, A.G., Heller, A. and Mullins, C.B., (2020). Sulfur-Rich Molybdenum Sulfide as a Cathode Material for Room Temperature Sodium-Sulfur Batteries. *ACS Appl. Energy Mater*. 3 (7), 6121-6126.

86. Yang, T., Guo, B., Du, W., Aslam, M.K., Tao, M., Zhong, W., Chen, Y., Bao, S.J., Zhang, X. and Xu, M. (2019). Design and Construction of Sodium Polysulfides Defense System for Room-Temperature Na–S Battery. *Adv. Sci*. 6 (23), 1901557.

87. Dong, C., Zhou, H., Jin, B., Gao, W., Lang, X., Li, J. and Jiang, Q. (2021). Enabling high-performance room-temperature sodium/sulfur batteries with few-layer 2H-$MoSe_2$ embellished nitrogen-doped hollow carbon spheres as polysulfide barriers. *J. Mater. Chem. A*. 9 (6), 3451-3463.

88. Pu, K.C., Zhang, X., Qu, X.L., Hu, J.J., Li, H.W., Gao, M.X., Pan, H.G. and Liu, Y.F. (2020). Recently developed strategies to restrain dendrite growth of Li metal anodes for rechargeable batteries. *Rare Met*. 39 (6), 616-635.

89. Yan, Z., Pan, H.Y., Wang, J.Y., Chen, R.S., Li, Q., Luo, F., Yu, X.Q. and Li, H., (2021). Enhancing cycle stability of Li metal anode by using polymer separators coated with Ti-containing solid electrolytes. *Rare Met*. 40 (6), 1357-1365.

90. Xu, C.X. and Jiang, J.J., (2021). Designing electrolytes for lithium metal batteries with rational interface stability. *Rare Met*. 40 (2), 243-245.

91. Fang, W., Jiang, R., Zheng, H., Zheng, Y., Sun, Y., Liang, X., Xiang, H.F., Feng, Y.Z. and Yu, Y., (2021). Stable sodium metal anode enhanced by advanced electrolytes with SbF_3 additive. *Rare Met*. 40 (2), 433-439.

92. Tang, X., Zhou, D., Li, P., Guo, X., Sun, B., Liu, H., Yan, K., Gogotsi, Y. and Wang,

G. (2020). MXene-Based Dendrite-Free Potassium Metal Batteries. *Adv. Mater*. 32 (4), 1906739.

93. Song, K., Liu, C., Mi, L., Chou, S., Chen, W. and Shen, C. (2021). Recent Progress on the Alloy-Based Anode for Sodium-Ion Batteries and Potassium-Ion Batteries. *Small*. 17 (9), 1903194.

94. Lee DJ, Park JW, Hasa I, Sun YK, Scrosati B, Hassoun J. (2013). Alternative materials for sodium ion-sulphur batteries. *J. Mater. Chem. A.* 1 (17), 5256-5261.

95. Bloi, L.M., Pampel, J., Dörfler, S., Althues, H. and Kaskel, S., (2020). Sodium Sulfide Cathodes Superseding Hard Carbon Pre-sodiation for the Production and Operation of Sodium–Sulfur Batteries at Room Temperature. *Adv. Energy Mater*. 10 (7), 1903245.

96. Yue, J., Han, F., Fan, X., Zhu, X., Ma, Z., Yang, J. and Wang, C. (2017). High-Performance All-Inorganic Solid-State Sodium-Sulfur Battery. *ACS Nano*. 11 (5), 4885-4891.

97. Wang, A., Hu, X., Tang, H., Zhang, C., Liu, S., Yang, Y.W., Yang, Q.H. and Luo, J., (2017). Processable and Moldable Sodium-Metal Anodes. *Angew Chem. Int. Ed*. 56 (39), 11921-11926.

98. Yang, T., Guo, B., Du, W., Aslam, M.K., Tao, M., Zhong, W., Chen, Y., Bao, S.J., Zhang, X. and Xu, M., (2019). Design and Construction of Sodium Polysulfides Defense System for Room-Temperature Na–S Battery. *Adv. Sci*. 6 (23), 1901557.

99. Hu, X., Ni, Y., Wang, C., Wang, H., Matios, E., Chen, J. and Li, W., (2020). Facile-Processed Nanocarbon-Promoted Sulfur Cathode for Highly Stable Sodium-Sulfur Batteries. *Cell Reports Phys. Sci*. 1 (2), 100015.

100. Hao Y, Li X, Sun X, Wang C. (2017). Nitrogen-Doped Graphene Nanosheets/S Composites as Cathode in Room-Temperature Sodium-Sulfur Batteries. *ChemistrySelect*. 2 (29), 9425-9432.

101. Du, W., Gao, W., Yang, T., Guo, B., Zhang, L., Bao, S.J., Chen, Y. and Xu, M., (2020). Cobalt nanoparticles embedded into free-standing carbon nanofibers as catalyst for room-temperature sodium-sulfur batteries. *J. Colld. Inter. Sci*. 565, 63-69.

102. Cameron, J.M., Holc, C., Kibler, A.J., Peake, C.L., Walsh, D.A., Newton, G.N. and Johnson, L.R., (2021). Molecular redox species for next-generation batteries. *Chem. Soc. Rev*. 50 (10), 5863-5883.

103. Wu, X., Liu, N., Guan, B., Qiu, Y., Wang, M., Cheng, J., Tian, D., Fan, L., Zhang, N. and Sun, K. (2019). Redox Mediator: A New Strategy in Designing Cathode for Prompting Redox Process of Li–S Batteries. *Adv. Sci*. 6 (21), 1900958.

104. Hwang and J-Y, Kim HM, Yoon CS, Sun Y-K. (2018). Toward High-Safety Potassium−Sulfur batteries using a polysulfide catholyte and metal-free anode. *ACS Energy Lett*. 3, 540-541.

105. Li L, Dai H, Wang C. (2020). Electrolyte additives: Adding the stability of lithium metal anodes. *Nano Sel*. 2, 16-36.

106. Liu X, Tan Y, Liu T, Wang W, Li C, Lu J. (2019). A Simple Electrode-Level Chemical Presodiation Route by Solution Spraying to Improve the Energy Density of Sodium-Ion Batteries. *Adv. Funct. Mater*. 29 (50), 1903795.

107. Zhao M, Li BQ, Zhang XQ, Huang JQ, Zhang Q. (2020). A Perspective toward Practical Lithium-Sulfur Batteries. *ACS Cent. Sci*. 6 (7), 1095-1104.

108. Cha E, Patel M, Bhoyate S, Prasad V, Choi W. (2020). Nanoengineering to achieve high efficiency practical lithium-sulfur batteries. *Nanoscale Horiz*. 5 (5), 808-831.

109. Ponraj R, Kannan AG, Ahn JH, Kim DW. (2016). Improvement of Cycling Performance of Lithium-Sulfur Batteries by Using Magnesium Oxide as a Functional Additive for Trapping Lithium Polysulfide. *ACS Appl. Mater. Interfaces*. 8 (6), 4000-4006.

110. Liu, H., Pei, W., Lai, W.H., Yan, Z., Yang, H., Lei, Y., Wang, Y.X., Gu, Q., Zhou, S.,

Chou, S. and Liu, H.K. (2020).Electrocatalyzing S Cathodes via Multisulfiphilic Sites for Superior Room-Temperature Sodium-Sulfur Batteries. *ACS Nano*. 14 (6), 7259-7268.

111. Chung SH, Manthiram A. (2017). Lithium-sulfur batteries with the lowest self-discharge and the longest shelf life. *ACS Energy Lett*. 2 (5), 1056-1061.

Figure legends

FIGURE 1 Motivation of the Research on Na-S and K-S Batteries. (A) Schematic of energy density of various batteries. (B) Schematic of comparison of abundance of different elements.

FIGURE 2 Reaction Mechanisms of Na-S Batteries. (A) Na-S phase diagram. Reproduced with permission from reference.[20] Copyright 2019,The electrochemical society. (B) Graph representing number of electrons transferred and cumulative specific capacity in Na-S batteries. (C) A typical discharge profile of S_8 in Na-S batteries. Reproduced with permission: Copyright 2014, Wiley-VCH.[19] (D) Charge-discharge voltage profile of small S in Na-S batteries. Reproduced with permission. Copyright 2013,Wiley-VCH.[21] (E) In-situ synchrotron XRD patterns of S_8/Co/hollow carbon for Na-S batteries. Reproduced with permission. Copyright 2018, Nature publishing group.[22]

FIGURE 3 Reaction Mechanism of K-S Batteries. (A) K-S phase diagram. Reproduced with permission from reference.[23] Copyright 2019, American chemical Society. (B) Graph representing number of electrons transferred and cumulative specific capacity in K-S batteries. Reproduced with permission: Copyright 2020, Wiley-VCH from reference. [13] (C) Charge-discharge profile of S_8 cathode in K-S batteries. (D) High resolution XPS S2p spectrum of S_8 discharged to 1 V. Reproduced with permission: Copyright 2018, Elsevier from reference.[30] (E) Charge-discharge profile of SPAN for K-S batteries. (F) High-resolution XPS S2p spectra

of SPAN discharged to 0.1 V. Reproduced with permission: Copyright 2018, Royal Society of Chemistry.[31]

FIGURE 4 Critical Challenges for Na-S and K-S Batteries. Cross-sectional images of PCNF/S cathode in the pristine state (A) and after cycles (B). Reproduced with permission from reference.[41] Copyright 2020, Royal society of Chemistry. (C) XRD patterns indicating the formation of K_2S_3 in the discharged state. Reproduced with permission: Copyright 2014. American Chemical Society.[36] (D) charge-discharge profiles of the first cycle of a K-S battery. Photographs of a K-S cell in OCV (E) and after discharging to 2.1 V (F). Reproduced with permission: Copyright 2019, Elsevier.[39]

FIGURE 5 Conductive Carbon Hosts for S_8. (A) SEM image of S/HMCS. Reproduced with permission: Copyright 2018, Elsevier.[42] (B),(C) TEM images of S/IHCS. Reproduced with permission: Copyright 2016, American Chemical Society.[43] (D) Digital photographic image of flexible CFC/S. Digital photographic image of pouch cell Na-S cell using CFC/S cathode (E) before bending, (F) after bending. Reproduced with permission: Copyright 2017, Elsevier.[44] (G) Rate performance of N-S co-doped PC/S. (H) Cyclic performance of N-S co-doped PC/S. Reproduced with permission: Copyright 2020, Wiley-VCH.[51]

FIGURE 6 Electrocatalytic Conversion of Sodium and Potassium Polysulphides. (A) Gibbs free energy diagram for the transformation between polysulfide intermediates on N-G and Co@N-G. (B) Density of states comparison between Co and N-G. (C) In-situ XRD patterns of Co-PCNF/S. Reproduced with permission: Copyright 2021, Wiley-VCH.[53] (D) Comparison of energy barrier of Co and N-Co for potassium polysulphide conversion. (E) Tafel plots for the oxidation and reduction reactions of polysulphides. Reproduced with permission: Copyright 2020, American Chemical society.[26]

FIGURE 7 Conductive Carbon Hosts for Small Sulphur Cathode. (A) Schematic illustration of the existing forms of sulfur in the porous carbon matrix and the electrochemical reaction to

form K_2S. Reproduced with permission: Copyright 2019, American chemical society.[62] (B) Schematic representation of discharge mechanism inside the micropore. Reproduced with permission: Copyright 2017, American Chemical Society.[59] (C) SEM image of microporous carbon sphere. Reproduced with permission: Copyright 2017, American Chemical Society.[59] (D) HRTEM image of CNT@MPC/S_2-S_4 Reproduced with permission: Copyright 2017, Wiley-VCH. [60] (E) CV curves of S_4@CS at 50 μV s^{-1}. Reproduced with permission: Copyright 2017, American Chemical society.[59] (F) Schematic illustration and voltage profile of CNT@MPC/S_2-S_4. Reproduced with permission: Copyright 2017, Wiley- VCH.[60] (G) High-resolution S 2p XPS spectrum of MPC/S_2-S_3 at a fully discharged state. Reproduced with permission: Copyright 2019, American Chemical society.[62]

FIGURE 8 Carbon Matrices for Covalent S Cathode. Schematic representation of the electrochemical reaction mechanism (A) and cycling performance of I-doped SPAN at 2 C for 500 cycles (B). Reproduced with permission: Copyright 2019, Royal society of Chemistry.[70] (C),(D) Ex-situ XRD patterns of C-S composites at different charge and discharged states in the 1st and 2nd cycle. Reproduced with permission: Copyright 2020, American Chemical Society.[73] (E) Synthesis of chemically bonded S in a microporous polymer PIM-1. (F) CE of S/PIM-1 cycled at 0.1 C for 250 cycles. Reproduced with permission: Copyright 2020. Royal Society of Chemistry.[72]

FIGURE 9 Catholytes for Na-S and K-S Batteries. (A) Schematic of a Na/dissolved polysulfide cell with a MWNT fabric electrode. (B) Discharge capacities as a function of cycle number for the cells with the dissolved sodium polysulfide/MWNT cathode and the conventional S-C cathode. Reproduced with permission: Copyright 2014, American Chemical Society.[74] (C) Schematic representation of preparation of CC@MnO_2/Na_2S_6. (D) Schematic representation of the possible interactions of manganese oxide with different sodium polysulfides and polythionate complexes. Reproduced with permission: Copyright 2018,

Elsevier.[75] (E) Initial charge−discharge profile of K-S cell using potassium polysulfide catholyte and potassium metal. (F) Charge-discharge profile of K-S cell using potassium impregnated HC anode and catholyte). Reproduced with permission: Copyright 2018, American Chemical Society.[76]

FIGURE 10 Carbon Composites as A Defence Layer to Control the Shuttling Effect. (A) SEM image of SWNTs coating on a Celgard separator. (B) Discharge capacities and CE as a function of cycle number for KSB with SWNTs coated and uncoated Celgard separator. Reproduced with permission: Copyright 2018, Elsevier.[30] (C) CE as a function of cycle number of CNF coated sodiated Nafion membrane. Reproduced with permission: Copyright 2016, American Chemical Society.[83] (D) Schematic representation of coating of HCS/MoS_2 on a glass fibre separator. Reproduced with permission: Copyright 2019, Wiley-VCH.[86] (E) Schematic representation of control of polysulfide shuttling using $MoSe_2$/NHCS/GO coated separator. Reproduced with permission: Copyright 2021, Royal Society of Chemistry.[87] (F) In-situ Raman analysis of the S@HCS/MoS_2 electrode at different states of charge. Reproduced with permission: Copyright 2019, Wiley-VCH.[86] (G) Calculated adsorption energies of soluble polysulphides on different materials. Reproduced with permission: Copyright 2021, Royal Society of Chemistry.[87]

FIGURE 11 Suppressing Dendrite Growth and Enriching the Mechanical Stability of Na and K Anodes **(**A) Schematic illustration of the synthesis of CNT@MXene/K scaffold. (B) Rate performance of the symmetric cells at different current densities. (C) Digital images and the corresponding UV–vis spectra of liquid electrolytes in optically transparent devices assembled with CNT@MXene/K anode (or bare K foil) and SPAN powder immersed in liquid electrolytes. Reproduced with permission: Copyright 2019, Wiley-VCH.[92] (D) Discharge capacity and CE of Na_2S cathode and hard carbon anode for a Na-S battery. Reproduced with permission: Copyright 2020, Wiley-VCH.[95] (E) Galvanostatic charge-discharge profiles of

$Na_{15}Sn_4$/C as the anode and Na_3PS_4-Na_2S-carbon composite cathode for a Na-S battery. Reproduced with permission: Copyright 2017, American Chemical Society.[96] (F) Digital image showing stacked Na pieces sticking together while Na@rGO pieces staying stacked together after compression. (G) SEM image of insoluble NaSx deposited on the surface of bare Na. Reproduced with permission: Copyright 2017, Wiley-VCH.[97]

Figure 1

Click here to access/download;Figure;Fig 1.tif

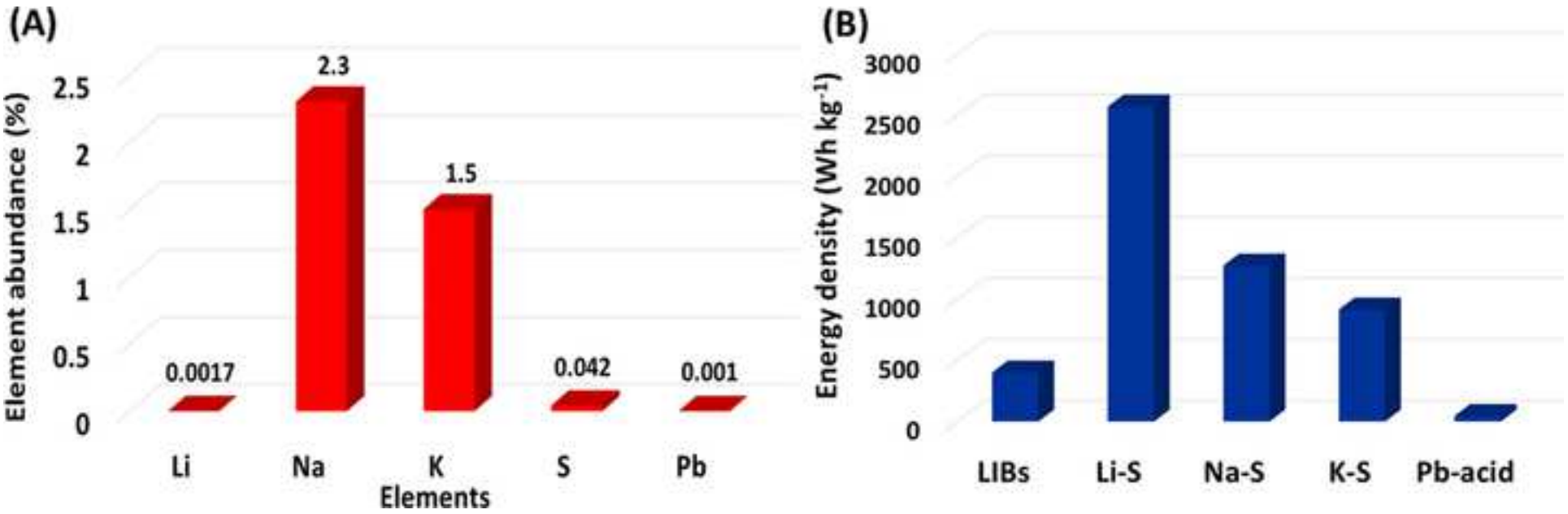

Figure 2

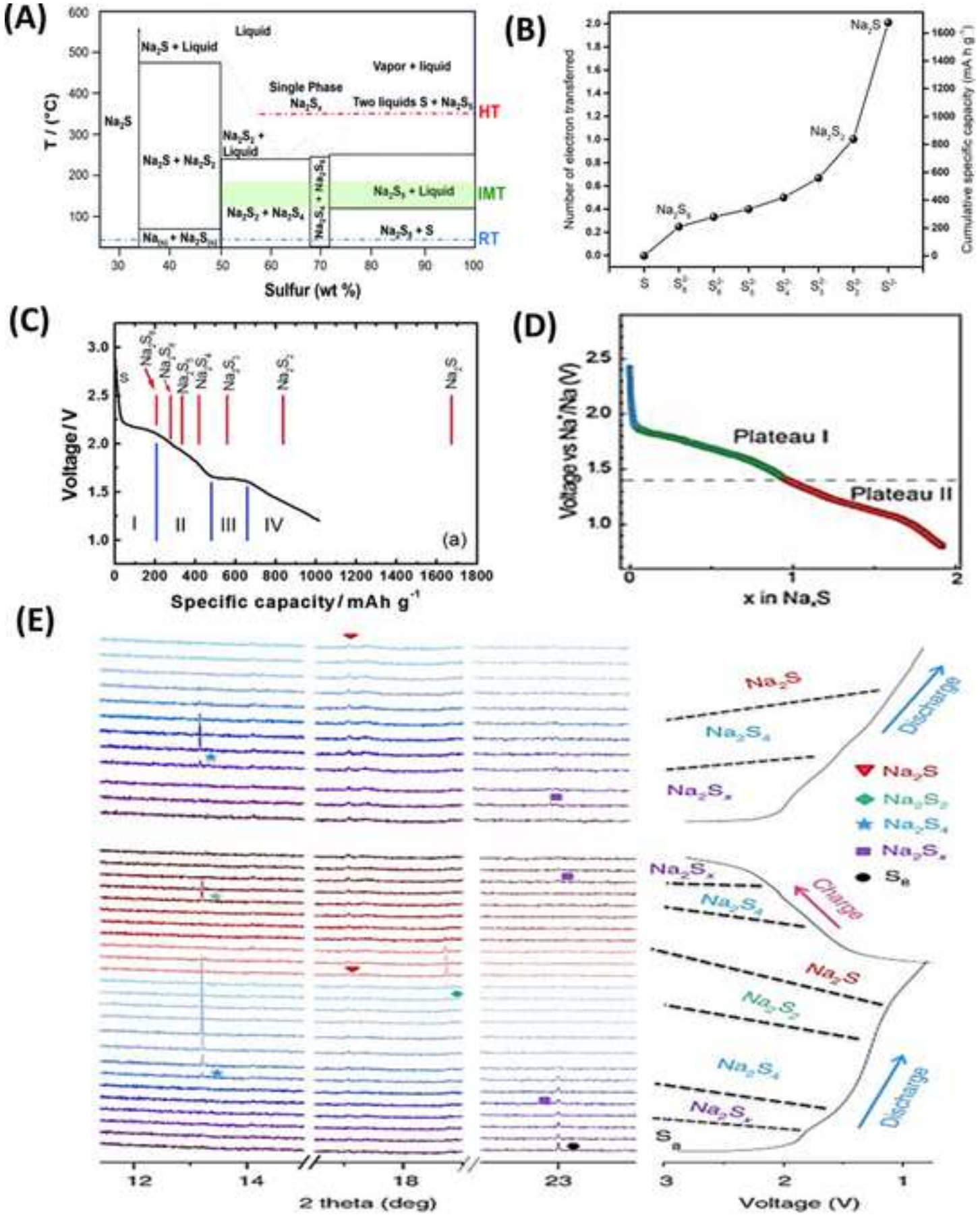

Figure 3

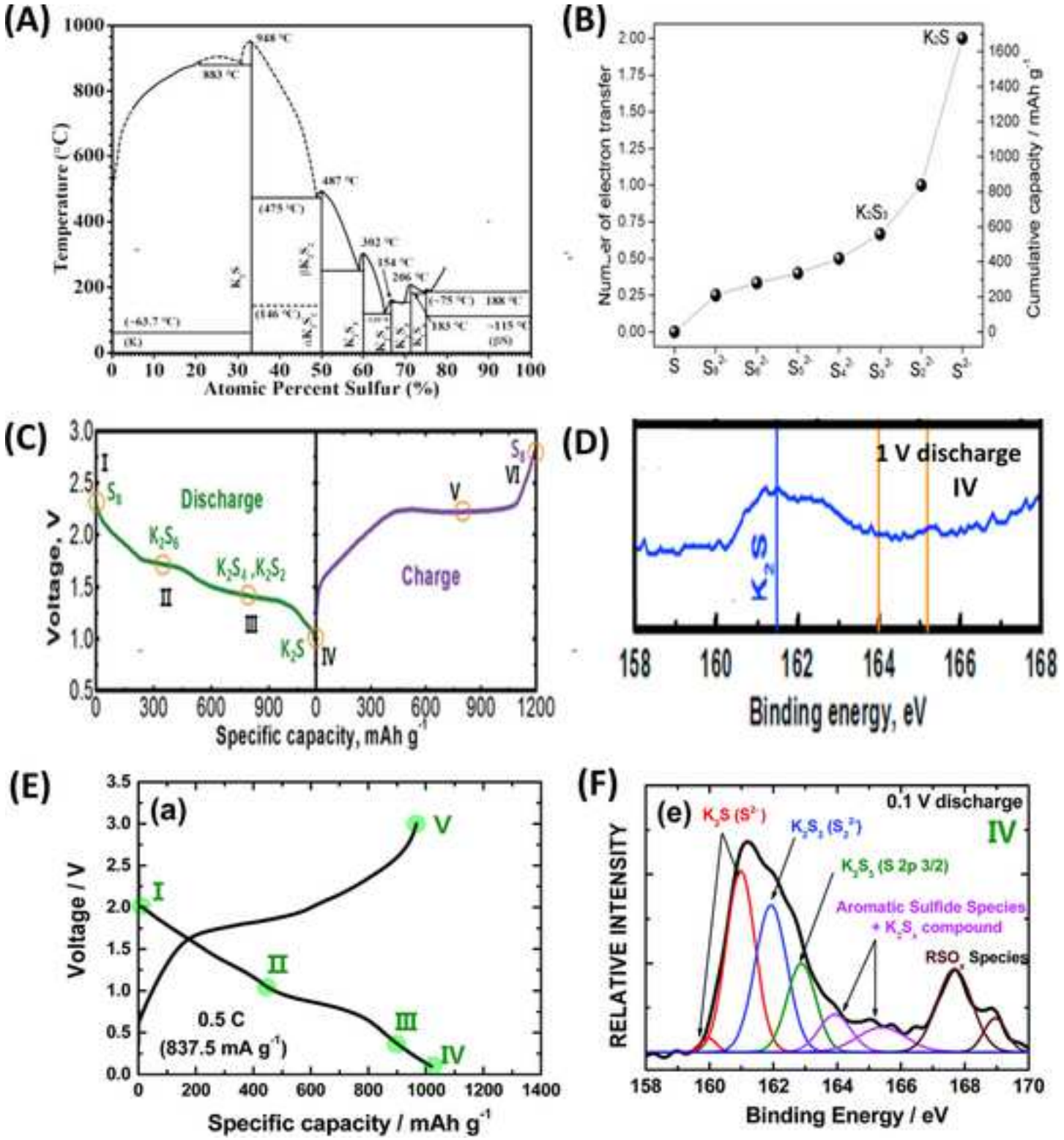

Figure 4

Click here to access/download;Figure;Fig 4.tif

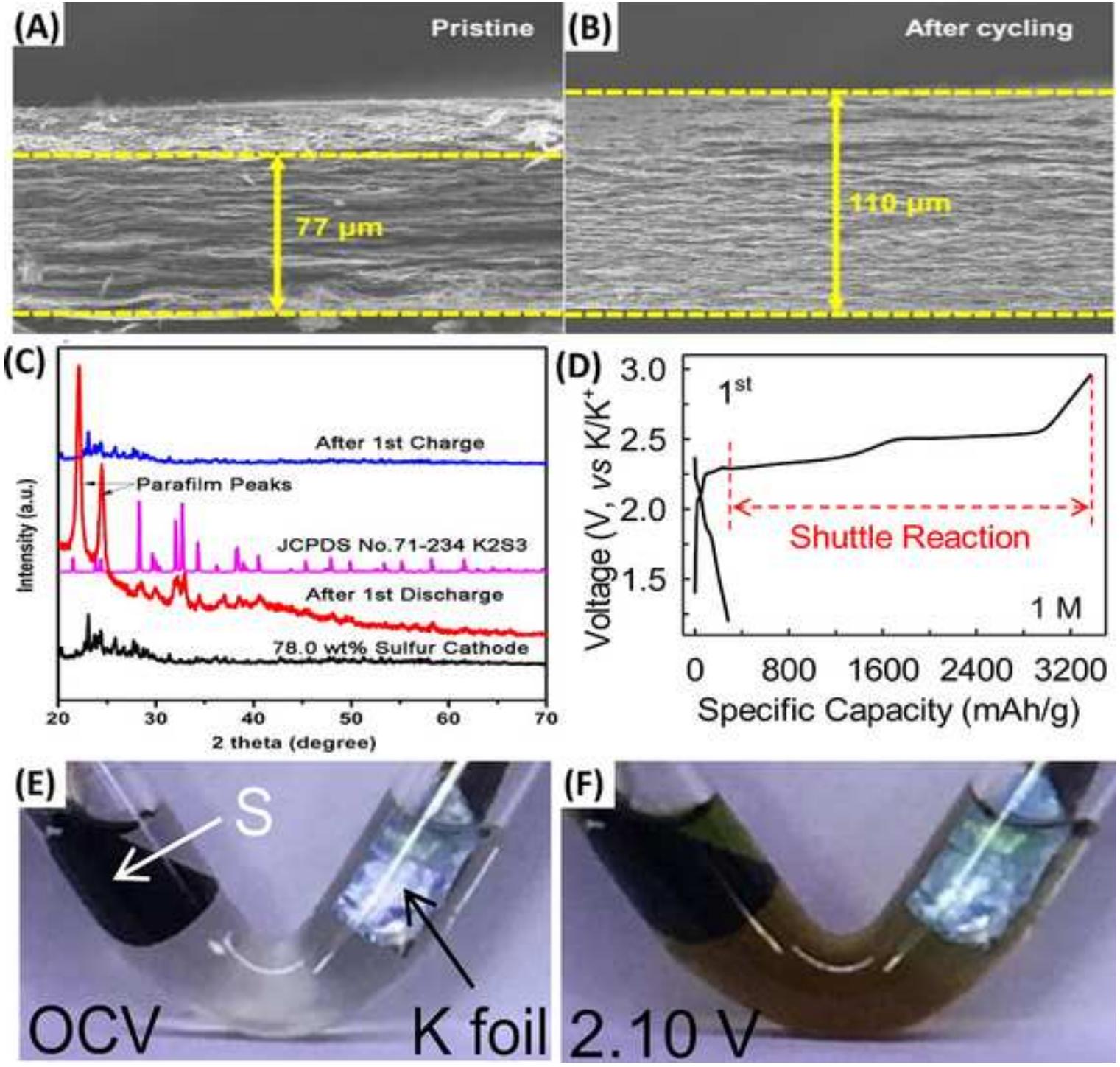

Figure 5

Click here to access/download;Figure;Fig 5.tif

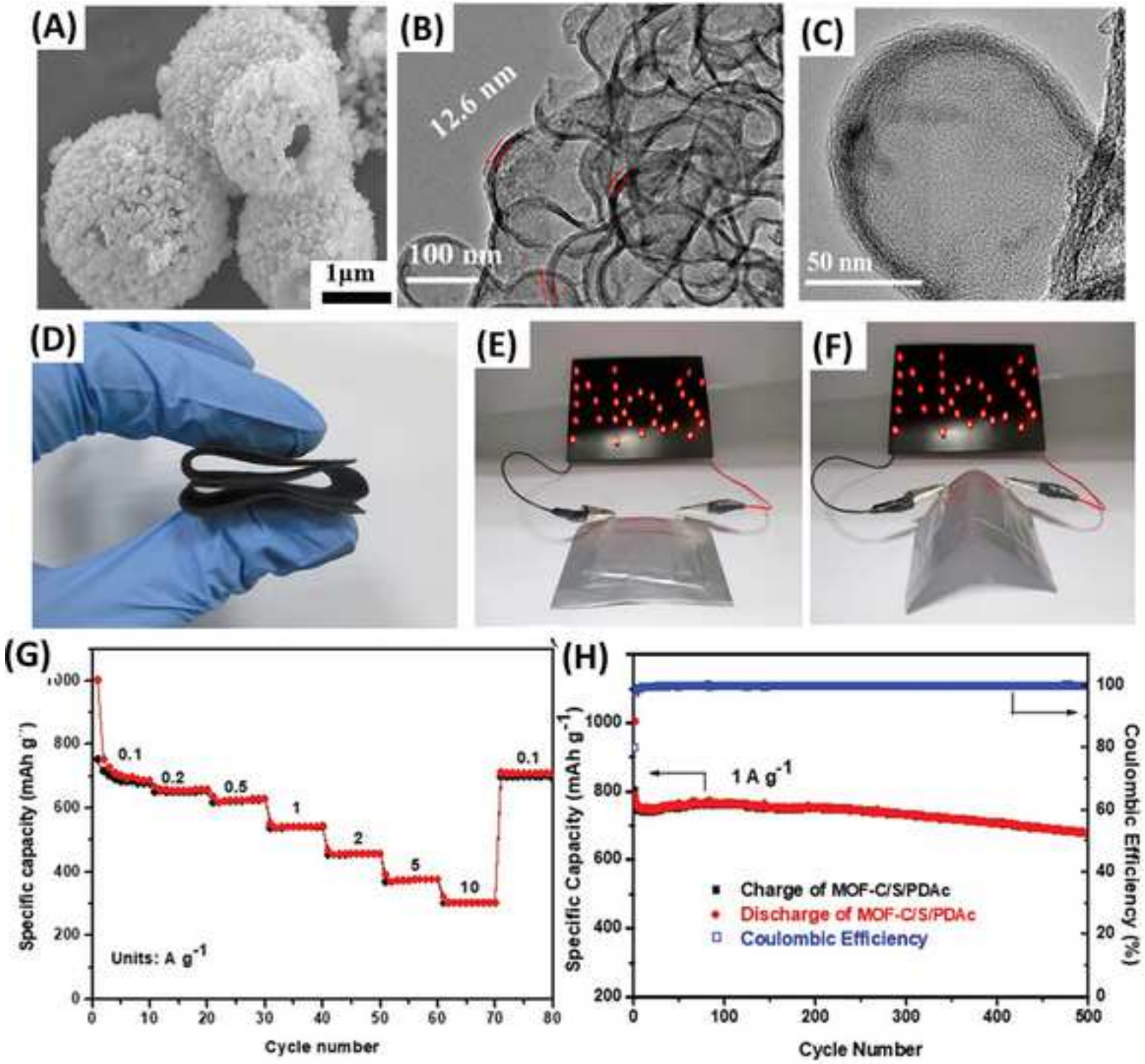

Figure 6

Click here to access/download;Figure;Fig 6.tif

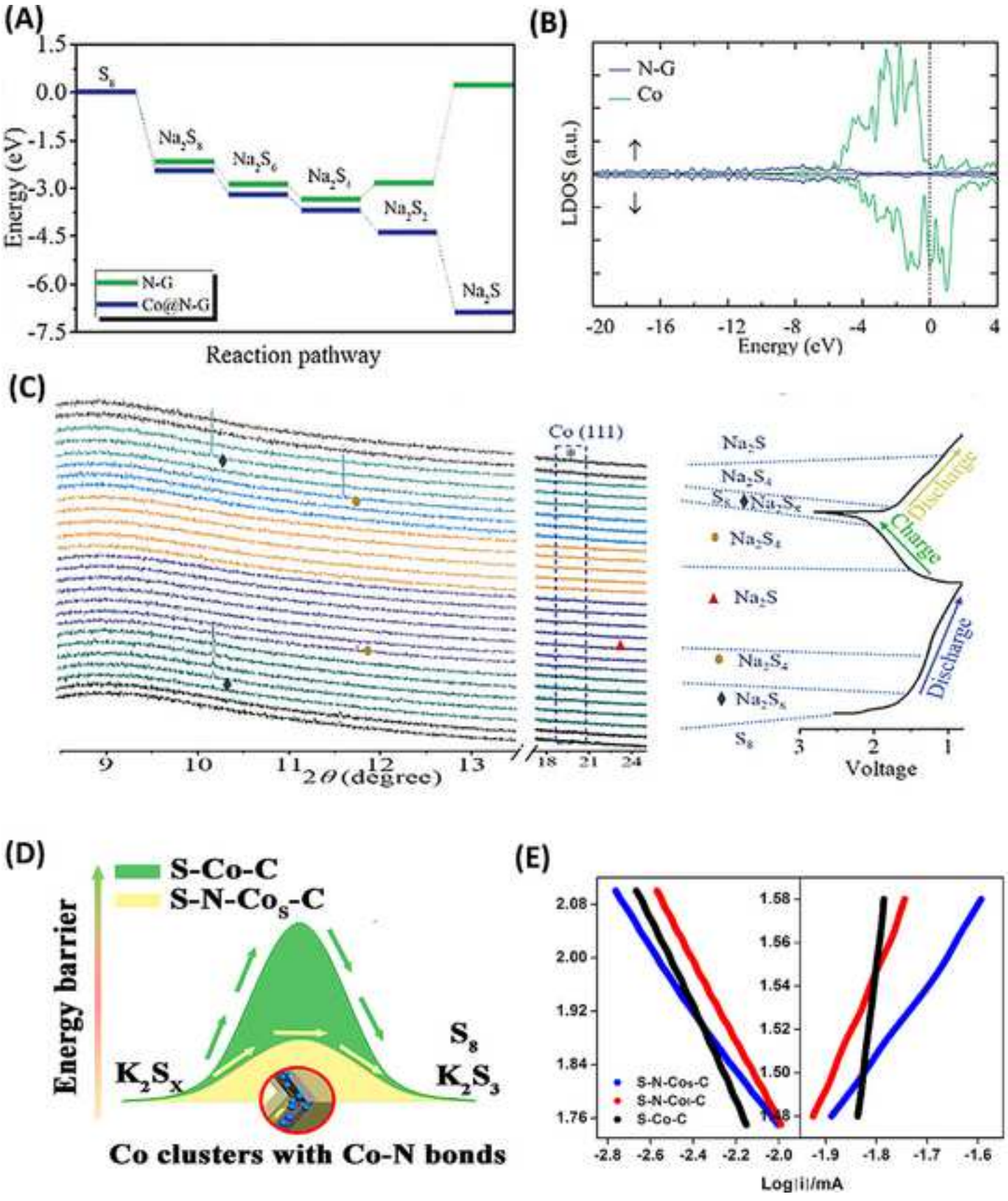

Figure 7

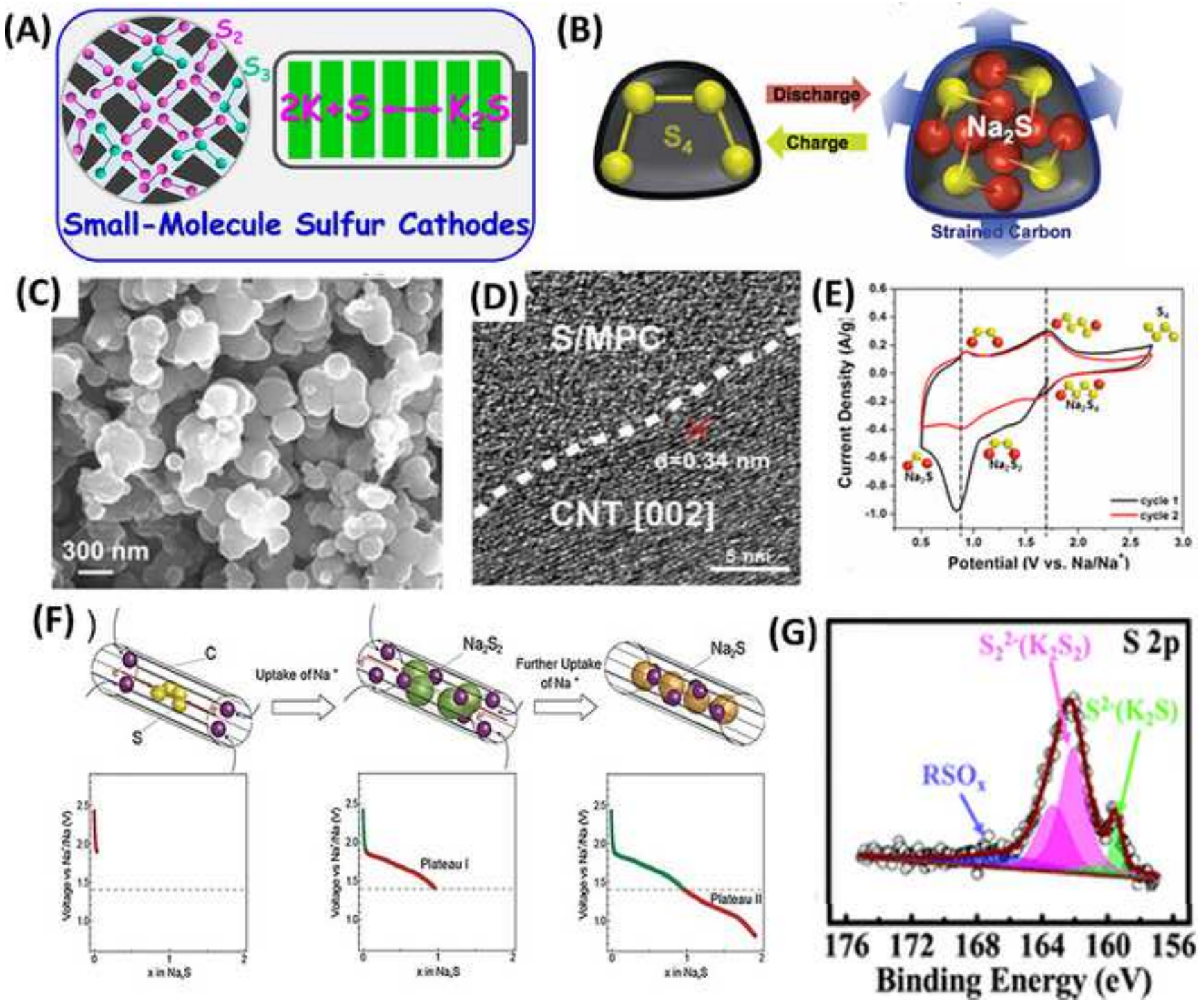

Figure 8

Click here to access/download;Figure;Fig 8.tif

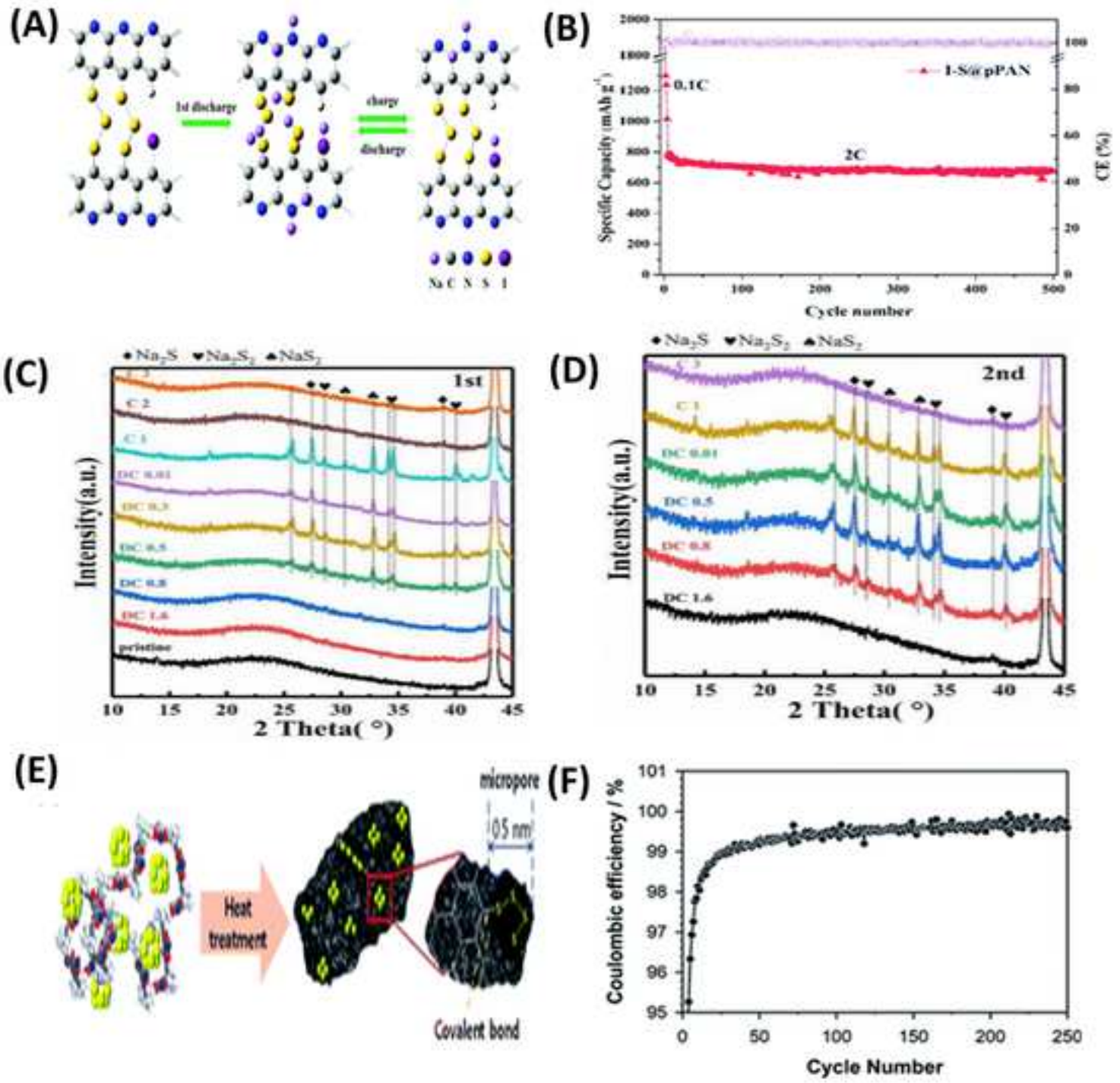

Figure 9

Click here to access/download;Figure;Fig 9.tif

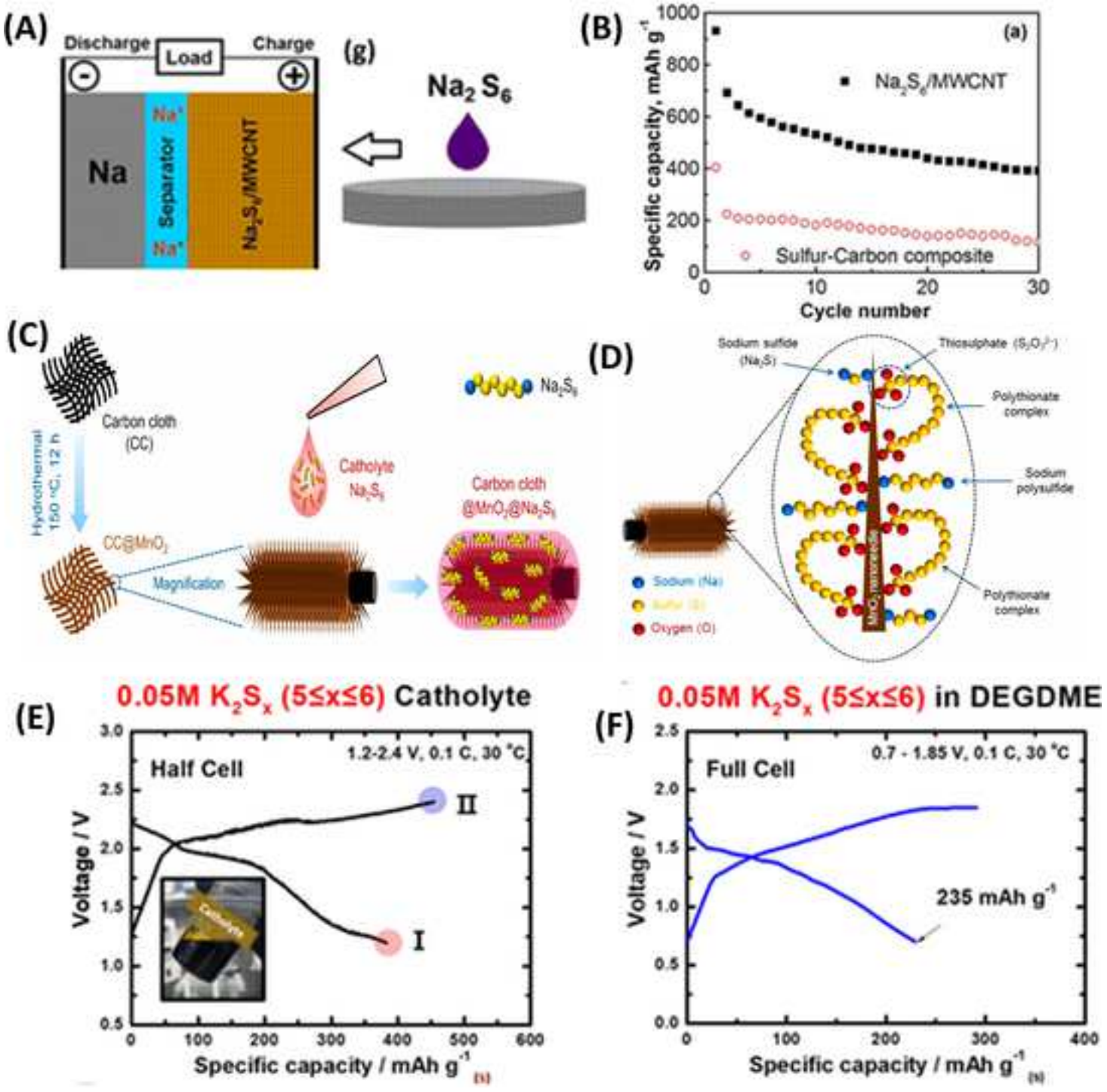

Figure 10

Click here to access/download;Figure;Fig 10.tif

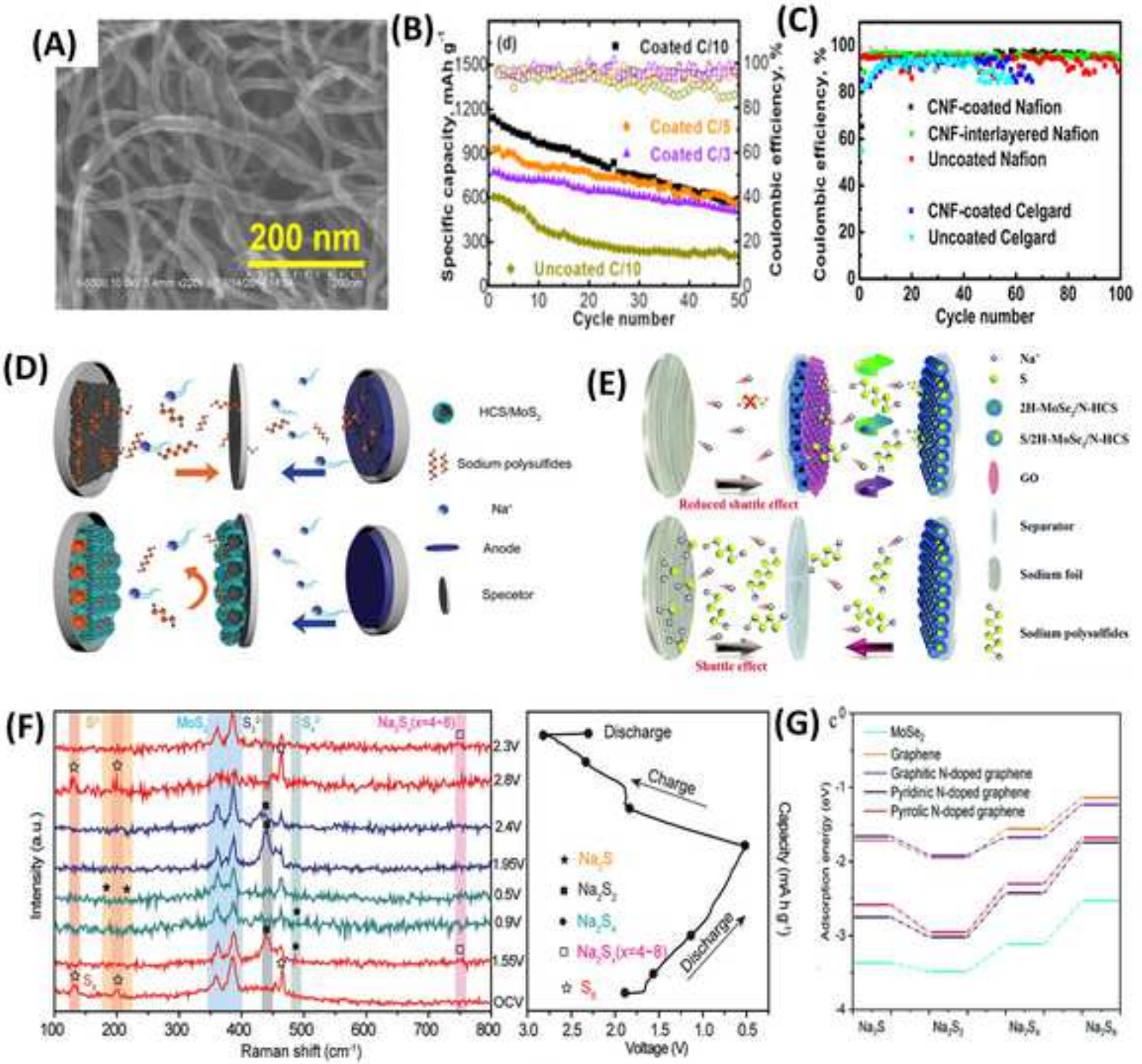

Figure 11